universe

MDPI

Review

From Barthel–Randers–Kropina Geometries to the Accelerating Universe: A Brief Review of Recent Advances in Finslerian Cosmology

Amine Bouali [1,2], Himanshu Chaudhary [3,4], Lehel Csillag [3,5], Rattanasak Hama [6], Tiberiu Harko [3,7,*], Sorin V. Sabau [8,9], Shahab Shahidi [10]

[1] Laboratory of Physics of Matter and Radiation, Mohammed I University, Oujda BP 717, Morocco; a1.bouali@ump.ac.ma
[2] Higher School of Education and Training, Mohammed I University, Oujda BP 717, Morocco
[3] Department of Physics, Babeș-Bolyai University, Kogălniceanu Street 1, 400084 Cluj-Napoca, Romania; himanshu.chaudhary@ubbcluj.ro; (H.C.); lehel.csillag@ubbcluj.ro (L.C.)
[4] Research Center of Astrophysics and Cosmology, Khazar University, 41 Mehseti Street, Baku AZ1096, Azerbaijan
[5] Department of Mathematics and Computer Science, Transilvania University, Iuliu Maniu Street 50, 500091 Brașov, Romania
[6] Faculty of Science and Industrial Technology, Prince of Songkla University, Surat Thani Campus, Surat Thani 84000, Thailand; rattanasak.h@psu.ac.th
[7] Astronomical Observatory, 19 Ciresilor Street, 400487 Cluj-Napoca, Romania
[8] School of Biological Sciences, Department of Biology, Tokai University, Sapporo 005-8600, Japan; sorin@tokai.ac.jp
[9] Graduate School of Science and Technology, Physical and Mathematical Sciences, Tokai University, Sapporo 005-8600, Japan
[10] School of Physics, Damghan University, Damghan 41167-36716, Iran; s.shahidi@du.ac.ir
* Correspondence: tiberiu.harko@aira.astro.ro

Abstract

We present a review of recent developments in cosmological models based on Finsler geometry, as well as geometric extensions of general relativity formulated within this framework. Finsler geometry generalizes Riemannian geometry by allowing the metric tensor to depend not only on position but also on an additional internal degree of freedom, typically represented by a vector field at each point of the spacetime manifold. We examine in detail the possibility that Finsler-type geometries can describe the physical properties of the gravitational interaction, as well as the cosmological dynamics. In particular, we present and review the implications of a particular implementation of Finsler geometry, based on the Barthel connection, and of the (α, β) geometries, where α is a Riemannian metric, and β is a one-form. For a specific construction of the deviation part β, in these classes of geometries, the Barthel connection coincides with the Levi–Civita connection of the associated Riemann metric. We review the properties of the gravitational field, and of the cosmological evolution in three types of geometries: the Barthel–Randers geometry, in which the Finsler metric function F is given by $F = \alpha + \beta$, in the Barthel–Kropina geometry, with $F = \alpha^2/\beta$, and in the conformally transformed Barthel–Kropina geometry, respectively. After a brief presentation of the mathematical foundations of the Finslerian-type modified gravity theories, the generalized Friedmann equations in these geometries are written down by considering that the background Riemannian metric in the Randers and Kropina line elements is of Friedmann–Lemaitre–Robertson–Walker type. The matter energy balance equations are also presented, and they are interpreted from the point of view of the thermodynamics of irreversible processes in the presence of particle creation. We investigate the cosmological properties of the Barthel–Randers and Barthel–Kropina cosmological models in detail. In these scenarios, the additional geometric terms arising from the Finslerian structure can

check for updates

Academic Editor: Antonino Del Popolo

Received: 29 April 2025
Revised: 14 June 2025
Accepted: 15 June 2025
Published: 20 June 2025

Citation: Bouali, A.; Chaudhary, H.; Csillag, L.; Harko, T.; Hama, R.; Sabau, V.S.; Shahidi, S. From Barthel–Randers–Kropina Geometries to the Accelerating Universe: A Brief Review of Recent Advances in Finslerian Cosmology. *Universe* **2024**, *11*, 198. https://doi.org/10.3390/universe11070198

Copyright: © 2024 by the authors. Licensee MDPI, Basel, Switzerland. This article is an open access article distributed under the terms and conditions of the Creative Commons Attribution (CC BY) license (https://creativecommons.org/licenses/by/4.0/).

be interpreted as an effective geometric dark energy component, capable of generating an effective cosmological constant. Several cosmological solutions—both analytical and numerical—are obtained and compared against observational datasets, including Cosmic Chronometers, Type Ia Supernovae, and Baryon Acoustic Oscillations, using a Markov Chain Monte Carlo (MCMC) analysis. A direct comparison with the standard ΛCDM model is also carried out. The results indicate that Finslerian cosmological models provide a satisfactory fit to the observational data, suggesting they represent a viable alternative to the standard cosmological model based on general relativity.

Keywords: Barthel connection; (α, β) metrics; Finslerian cosmology; posterior inference; MCMC statistical analysis

1. Introduction—Early History and Modern Developments

In 1918, the same year in which Herman Weyl proposed his important extension of Riemannian geometry [1,2], by introducing the concept of non-metricity to mathematics and physics, another equally interesting generalization of the Riemannian framework was proposed by Paul Finsler [3]. The work of Weyl was clearly influenced by the progresses in the physics of his time, and especially by the development of general relativity by Einstein [4,5] and Hilbert [6], and it has been extensively used in physics, especially recently [7]. On the other hand, Finsler geometry, which represents, at least from a physicist's perspective, a much more drastic extension of Riemannian geometry, was not considered from the point of view of applications in fundamental physics for at least 40 years.

Actually, Finslerian geometry was already anticipated by Riemann [8], who already assumed the existence of metric structures in a general space based on the distance element $ds = F\left(x^1, x^2, \ldots, x^n; dx^1, dx^2, \ldots, dx^n\right) = F\left(x^1, x^2, \ldots, x^n;, y^1, y^2, \ldots, y^n\right)$, or simply $F(x, y)$, where the condition that for $y = 0$, F is a positive definite function defined on the tangent bundle TM must also be imposed. In order to assure the independence of the length of curves on their parameterization, it is further required that F is a homogeneous function of degree one in y. Riemann geometry is just a special case of the general distance element ds, obtained under the assumption $F^2 = g_{IJ}(x)dx^I dx^J$. Thus, Finsler geometry is not a proper generalization of Riemann's geometry, but it "...is just Riemannian geometry without the quadratic restriction" [9]. However, it is an established practice especially in the physics literature to describe Finsler geometry as a generalization of Riemann's geometry, and in the present work, we will also adopt this view, mostly for the simplicity of the presentation.

In a simple description, Finsler geometry can be considered as a geometry in which the metric tensor g_{ij} is a function of both the coordinates x, defined on the base manifold M, and of the tangent vectors y, so that $g_{IJ} = g_{IJ}(x, y)$. In a physically intuitive sense, Finsler geometry can be considered as a geometry in which the metric tensor, determining the distance between two neighboring points, is an arbitrary function of both coordinates and velocities. For presentations of Finsler geometry from a mathematical perspective, see [10–13].

The remarkable success of general relativity in the description of gravitational phenomena and its many observational confirmations have significantly strengthened the position of Riemannian geometry as the "true" geometry of nature. General relativity, in its Riemannian formulation, successfully passes all the Solar System tests, inside which it can explain the gravitational phenomenology with high precision. Important confirmations of the validity of general relativity include such diverse phenomena as the perihelion precession of Mercury, light bending by the Sun, frame dragging, the Nordtvedt effect in

lunar motion, and the Shapiro time delay [14]. The experimental detection of gravitational waves represents a brilliant confirmation of the predictions of general relativity [15], which opened a new window in the Universe, and led to new perspectives on the black hole properties, their dynamical evolution, and the mass distribution of neutron stars [16]. Inspired by the immense success of general relativity, the Riemannian geometric framework was also extended, leading to important developments in mathematics like the introduction of the concept of torsion [17,18], or of the concept of absolute parallelism [19]. These new geometries have found important applications in physics, and they have been used to model the gravitational interaction from new perspectives.

From a mathematical point of view, Ehlers Pirani and Schild aimed to develop a constructive axiomatization of gravity. In their seminal 1972 paper, they built up the kinematical structure of general relativity, purely based on axioms, which have a somewhat empirical content [20]. Although the axiomatization is quite dense and technical, recent pedagogical reviews are present in the literature [21–23]. We briefly outline the four steps of the axiomatization in the following [24]:

1. In the first step, the basic physical/empirical entities are postulated, such as the timelike worldlines for freely falling massive particles, the lightlike worldlines of light rays, and radar echoes between massive particle worldlines. These empirical elements provide enough structure to define a system of coordinates and allow for the construction of a differentiable structure on the spacetime set M, turning it into a smooth manifold.
2. The conformal structure is established by requiring that, at each point in spacetime, the set of all possible directions (i.e., tangent vectors) splits into two components when the directions corresponding to massless (lightlike) trajectories are removed. This splitting reflects the causal distinction between future and past. Additionally, in a sufficiently small neighborhood V around the worldline of a massive particle, for any point $p \in V$ not lying on the particle's path, the function that maps p to the product of the radar emission time t_e and reception time t_r, i.e., $p \mapsto t_e t_r$, must be at least twice differentiable.
3. Imposing that through each point in spacetime, and for each timelike direction, there exists one unique timelike (massive) trajectory passing through that point, which results in a projective structure. Each of these trajectories must admit a parametrization such that, in local coordinates near the point, the motion satisfies $\ddot{x} = 0$. This expresses the fact that particles move along straight lines in free fall.
4. In the final step, compatibility between the conformal and projective structures is required. In particular, light rays must be special cases of particle geodesics in the limit of zero mass. This determines the metric up to a conformal factor, which leads to a Weyl structure. Through some technical steps, eliminating the second clock effect leads to a Lorentzian structure, i.e., a pseudo-Riemannian manifold.

It turns out that if one weakens the twice differentiability assumption on the map $p \mapsto t_e t_r$, there are Finsler functions which satisfy all the other EPS axioms. A well-known example is given by

$$F(x,y) = e^{2\sigma(x,y)} \sqrt{|a_{IJ}(x) y^I y^J|}, \tag{1}$$

where $\sigma(x,y)$ is a non-singular 0-homogeneous function in y satisfying

$$\partial_K \sigma - y^M \Gamma^N_{MK}(x) \frac{\partial \sigma(x,y)}{\partial y^N} = 0, \tag{2}$$

with Γ^N_{MK} being the Christoffel symbols associated with the Riemannian metric $a_{IJ}(x)$. This geometry is of Berwald type, i.e., it is the closest to a Riemannian geometry, but it is not trivial.

Despite the systematic, rigorous and physically appealing nature of Finsler geometry, the applications in physics of this geometry appeared relatively late. A first step in this direction was taken in the work of Randers [25], who tried to formulate a unified theory of electromagnetism and gravity. Initially, the theory was formulated in a higher-dimensional Riemannian geometry. The Finslerian nature of the Randers geometry was recognized by Ingarden [26]. Essentially, Randers geometry is a specific example of a Finsler geometry, with the fundamental function $F(x,y) = \left(a_{IJ}(x)dx^I dx^J\right)^{1/2} + b_K(x)y^K$, where $b_K(x)$ is an arbitrary vector field. Presently, Randers spaces are considered as Finsler spaces $F^n = (M, \alpha + \beta)$, equipped with the Cartan nonlinear connection N, i.e., they are denoted with $RF^n = (M, \alpha + \beta, N)$ [27]. A comprehensive overview of several Finsler metrics and of some of their physical applications is given in Table 1.

Table 1. Examples of Finsler metrics with their defining functions and characteristic properties.

Name	Finsler Function $F(x,y)$	Properties
Semi-Riemannian	$F(x,y) = \sqrt{\lvert a_{IJ}(x)y^I y^J \rvert}$	Quadratic in y, reversible, i.e., $F(x,y) = F(x,-y)$.
Randers	$F(x,y) = \sqrt{a_{IJ}(x)y^I y^J} + b_I(x)y^I$	Non-reversible, i.e., $F(x,y) \neq F(x,-y)$; appears in EM analogs and Lorentz-violating physics.
Kropina	$F(x,y) = \frac{a_{IJ}y^I y^J}{b_I y^I}, \quad b_I y^I \neq 0$	Singular on hypersurfaces; non-reversible.
Matsumoto	$F(x,y) = \frac{\sqrt{a_{IJ}y^I y^J}}{\sqrt{a_{IJ}y^I y^J} - b_K y^K}$	Non-reversible; used in irreversible mechanics; singular on hypersurfaces.
Bogoslovsky	$F(x,y) = \left(-\eta_{IJ}y^I y^J\right)^{\frac{1-b}{2}} \left(n_K y^K\right)^b$	Breaks full Lorentz invariance; $0 < b < 1$; used in very special relativity.
Funk	$F(x,y) = \frac{\sqrt{\delta_{IJ}y^I y^J} - \delta_{IJ}x^I y^J}{1 - \delta_{IJ}x^I x^J}$	Defined on unit ball; forward complete; non-reversible.
Locally Minkowskian	$F(x,y) = F(y)$	General flat case; depends only on y, independent of x.
α-β metrics	$F = \phi(\alpha,\beta), \quad \alpha = \sqrt{a_{IJ}y^I y^J}, \ \beta = b_K y^K$	Unifies and generalizes Randers, Kropina, and Matsumoto metrics via the scalar function ϕ.
General Lagrangian	$F(x,y) = \sqrt{L(x,y)}$, L 2-homogeneous in y	More general case; has some applications in mechanics.
Optical/media	$F(x,y) = n(x,y)\lVert y \rVert$	Includes anisotropic effects in optics through the direction-dependent refractive index $n(x,y)$.
Non-reversible Finsler	General F such that $F(x,y) \neq F(x,-y)$	Includes Funk, Randers, and non-reversible geometries.

Finsler geometry has found applications in several areas of physics, including the geometric formulation of quantum mechanics [28–31], kinetic theory of gases [32,33], dispersion relations [34] and optics [35]. A more exotic application is related to an extension of the standard model of particle physics, where a Finsler structure can be given for the nonminimal fermion sector [36]. It is also interesting to note that Lorentz-violating scalar fields can also be described by Riemann–Finsler geometry [37]. In the latter cases, the Finsler geometry considered is of Berwald type: the closest one to the Riemannan geometry, which is still not trivial and compatible with the weakened Ehlers–Pirani–Schild axioms.

The first attempts at formulating a Finslerian theory of gravitation, but still in the framework of unified field theories, belonged to Horváth [38], and Horváth and Moór [39].

Early Finslerian-type gravitational theories were also formulated in [40,41], where a set of Finslerian-type gravitational field equations were proposed, representing a straightforward extension of the Einstein field equations, and given by

$$R_{\mu\nu} - \frac{1}{2}g_{\mu\nu}R + \lambda g_{\mu\nu} = \chi T_{\mu\nu}, K_{\mu\nu} - \frac{1}{2}g_{\mu\nu}K + \lambda g_{\mu\nu} = \chi T_{\mu\nu}, \tag{3}$$

and

$$S_{\mu\nu} - \frac{1}{2}g_{\mu\nu}S - \lambda^{(i)}g_{\mu\nu} = -\chi^{(i)}T^{i}_{\mu\nu}, \tag{4}$$

respectively. In Equations (3) and (4), χ denotes the gravitational constant, λ is the cosmological constant, and $\lambda^{(i)}$ and $\chi^{(i)}$ represent the internal cosmological and gravitational constants. The quantities $R_{\mu\nu}$, R, $K_{\mu\nu}$, K and $S_{\mu\nu}$ and S denote the hh-, hv- and vv-Ricci curvature tensors, and the hh-, hv- and vv-scalar curvatures of the Finsler space (M, F). Moreover, $T_{\mu\nu}$ is the energy–momentum tensor of the baryonic matter, and $T^{i}_{\mu\nu}$ denotes the internal energy–momentum tensor. In [42] another Finslerian-type approach to gravity was introduced and developed. The main focus of this work was the Finslerian description and interpretation of the particle motion in a gravitational field. For the Finslerian extensions of general relativity along the line of [42], see [43]. Finslerian-type generalized Schwarzschild metrics have been investigated in [44,45]. For further studies of black holes and wormholes in Finsler geometry, see [46–55].

Miron [56] has proposed the vector bundle point of view to formulate a system of Einstein-type gravitational field equations. The starting point of this approach is to interpret the field y as a fiber at the point x of the base manifold M. The total space of this vector bundle is obtained as a unification of the fields x and y [57]. A nonlinear connection naturally induces an adapted basis in the fiber $T_{(x,y)}TM$ of the double tangent bundle TTM and a corresponding dual basis in the fiber $T^{*}_{(x,y)}TM$ of the cotangent bundle $T^{*}TM$. These are given by

$$X_A = \left(\frac{\delta}{\delta x^{\lambda}} = \frac{\partial}{\partial x^{\lambda}} - N^{i}_{\lambda}\frac{\partial}{\partial y^{i}}, \frac{\partial}{\partial y^{i}}\right), X^{A} = \left(dx^{\kappa}, \delta y^{i} = dy^{i} + N^{i}_{\lambda}dx^{\lambda}\right), \tag{5}$$

respectively.

In Equation (5), the indices A, B run over $(A, B) \in \{0, 1, 2, 3, ..., 7\}$, while the Greek indices λ, κ take values in $\{0, 1, 2, 3\}$. The functions N^{i}_{λ} define the nonlinear connection. By construction, the basis (5) is adapted to a Finsler-type metric on TM, given by

$$G = g_{\lambda\kappa}(x, y)dx^{\kappa}dx^{\lambda} + g_{ij}(x, y)\delta y^{i}\delta y^{j}, \tag{6}$$

where $g_{\lambda k}(x, y)$ and $g_{ij}(x, y)$ are the horizontal and vertical metric components, respectively.

In the total space of the vector bundle, the Einstein field equations are assumed to have their standard general relativistic form, $\mathcal{R}_{AB} - (1/2)\mathcal{R}g_{AB} = \tau_{AB}$, where τ_{AB} is the matter energy–momentum tensor. The field equations can be decomposed, and can be written as [56]

$$R_{\lambda\nu} - \frac{1}{2}(R + S)g_{\lambda\nu} = \tau_{\lambda\nu}, \overset{1}{P}_{i\lambda} = \tau_{i\lambda}, \overset{2}{P}_{\lambda i} = -\tau_{\lambda i}, \tag{7}$$

$$S_{ij} - \frac{1}{2}(R + S)g_{ij} = \tau_{ij}. \tag{8}$$

An interesting Finslerian-type gravitational theory was proposed in [58]. The basic idea of this approach is the assumption that the Einstein vacuum field equations can be

obtained from the condition $H = H^i_i = 0$, where H^i_k, the Finslerian deviation tensor, is obtained from the first and second derivatives of the quantity $G^l = \gamma^l_{jk}\dot{x}^j\dot{x}^k/2$ as

$$H^i_{\ k} = 2\frac{\partial G^i}{\partial x^k} - \frac{\partial^2 G^i}{\partial x^j \partial \dot{x}^k}\dot{x}^j + 2\frac{\partial^2 G^i}{\partial \dot{x}^j \partial \dot{x}^k}G^j - \frac{\partial G^i}{\partial \dot{x}^j}\frac{\partial G^j}{\partial \dot{x}^k}. \tag{9}$$

If the metric is Riemannian, we obtain the limiting case of the general relativistic gravitational field equations. But Finslerian solutions of the gravitational field equations proposed in [58] can also be obtained.

An important class of Finsler geometries is represented by Berwald–Finsler spaces. A system of gravitational field equations defined in a Berwald geometry was proposed and investigated in [59]. The derivation of the field equations in the Berwald–Finsler geometry is essentially based on the Bianchi identities satisfied by the Chern curvature tensor. In general, the geometric part of the gravitational field equation is not symmetric, and this indicates that the principle of the local Lorentz invariance is not satisfied in this theory. The field equations as proposed in [59] are given by

$$\left[Ric_{\mu\nu} - \frac{1}{2}g_{\mu\nu}S\right] + \left\{\frac{1}{2}B_{\alpha\ \mu\nu}^{\ \alpha} + B_{\mu\ \nu\alpha}^{\ \alpha}\right\} = 8\pi G T_{\mu\nu}, \tag{10}$$

where

$$A_{\lambda\mu\nu} \equiv \frac{F}{4}\frac{\partial}{\partial y^\lambda}\frac{\partial}{\partial y^\mu}\frac{\partial}{\partial y^\nu}(F^2), \tag{11}$$

is the Cartan tensor, and $B_{\mu\nu\alpha\beta} = -A_{\mu\nu\lambda}R^{\lambda}_{\theta\ \alpha\beta}y^\theta/F$. The Cartan tensor measures the deviation of the Finsler geometry from the Riemannian one on a given manifold.

With the use of a variational principle, Finsler-type gravitational field equations have been derived from a Finsler–Lagrange function L in [60]. The action considered in [60] is given by

$$S[L] = \int_{\Sigma\subset TM} \mathrm{vol}(\Sigma)R_{|\Sigma}, \tag{12}$$

where $\Sigma = \{(x,\dot{x}) \in TM | F(x,\dot{x}) = 1\}$ denotes the unit tangent bundle, and $\mathrm{vol}(\Sigma)$, the volume form on Σ, is defined by using the Finsler metric. The field equations obtained from the action (12) are given by

$$2R - \frac{L}{3}g^{Lij}R_{.i.j} + \frac{2L}{3}g^{Lij}\left[(\nabla P_i)_{\cdot j} + P_{i|j} - P_iP_j\right] = 0, \tag{13}$$

where P is the Landsberg tensor, and

$$g^L_{ij} = \frac{1}{2}\frac{\partial^2 L}{\partial \dot{x}^i \partial \dot{x}^j} = \frac{1}{2}L_{.i.j}. \tag{14}$$

Moreover, $R_{.i.j}$ is the geodesic deviation operator, and R denotes its trace.

When extended to gravitational systems much bigger than the Solar System, which involve the presence of galactic and cosmological scales, Einstein's theory of general relativity faces a number of very serious challenges, whose possible solutions could be obtained only if we introduce a fundamental modification in our understanding of the gravitational force.

One of the most intriguing discoveries of the recent times is the observational proof that our Universe is in fact in a phase of accelerating expansion [61–65]. The transition from deceleration to acceleration occurred at a small redshift z, given by $z \approx 0.5$. Explaining this observation requires a profound modification of the theoretical foundations of Einstein's general relativity.

The simplest explanation of the recent exponential de Sitter-type expansion can be obtained by reintroducing the cosmological constant Λ in the Einstein field equations, introduced by Einstein in 1917 [66], and later rejected by him as the biggest blunder of his life. Einstein's main goal was to use Λ to construct a static, general relativistic cosmological model of the Universe.

The cosmological constant has a complicated history [67], but presently, it is adopted as one of the basic physical (geometrical?) parameters to build up the standard cosmological paradigm, the ΛCDM model, which is currently used for the interpretation of the observational data. The ΛCDM model also includes in its theoretical structure another basic, equally mysterious component, dark matter [68]. Intensive searches for the dark matter particle have yielded no results, and thus, the only evidence for the existence of dark matter is gravitational. However, despite these theoretical shortcomings, the ΛCDM model fits the observational data very well [69–72].

But on the theoretical level, the ΛCDM model is confronted with the uncertainty of its foundations: no (convincing) physical theory exists that could provide it with a solid basis. The first major problem is related to the geometrical or physical interpretation of the cosmological constant [67,73,74]. If we interpret the cosmological constant as the vacuum energy density ρ_{vac} at the Planck scale, we are led to the "worst prediction in physics" [75]. The vacuum energy density can be computed as

$$\rho_{vac} \approx \frac{\hbar}{c}\int_{k_{dS}}^{k_{Pl}} \sqrt{k^2+\left(\frac{mc}{\hbar}\right)^2}\, d^3k \approx \rho_{Pl} = \frac{c^5}{\hbar G^2} = 10^{93}\ \frac{\mathrm{g}}{\mathrm{cm}^3}, \tag{15}$$

and this result differs by a factor of 10^{-120} from the observed value of the energy density associated with Λ, $\rho_\Lambda = \Lambda c^2/8\pi G \approx 10^{-30}$ g/cm^3 [71].

Presently, the ΛCDM standard paradigm is faced with several important problems. An important challenge to the ΛCDM model is the "Hubble tension", which has its origins in the differences in the estimations of the values of the Hubble constant H_0 (representing the present-day value of the Hubble function H), obtained on one hand from the CMB measurements [72], and on the other hand from the local observations of the Type Ia Supernovae [76–78]. The value of H_0 obtained by the SHOES collaboration for H_0 is $H_0 = 74.03 \pm 1.42$ km/s/Mpc [76]. The early Universe determinations, using the Planck satellite data, give for H_0 the value $H_0 = 67.4 \pm 0.5$ km/s/Mpc [72], which differs by $\sim 5\sigma$ from the SH0ES estimations.

Several other theoretical problems whose solution cannot be found in the framework of the ΛCDM paradigm still exist. Some of these problems are represented by the question of the smallness of Λ and its fine tuning. The question of why the transition from the decelerating to the accelerating phases took place recently is still waiting for a response. And perhaps the most important question, if the cosmological constant is really required to construct successful cosmological models, does not have an answer yet.

Hence, considering alternative approaches for the description of the gravitational interaction may allow us to solve the observational problems of cosmology, and reconsider the cosmological constant from a new perspective. There are three major possibilities that have been proposed for the extension of general relativity: the dark component approach, the dark gravity approach, and the dark coupling approach [79]. In the dark gravity approach, it is assumed that the geometry of the Universe, as well as the description of the gravitational interaction, requires a significant departure from the formalism of the Riemann geometry. Geometries that go beyond the Riemannian one, for example, Weyl geometry, geometries with torsion, or teleparallel geometries, have been investigated in [80–90]. For reviews of dark gravity-type theories, and their applications, see [91–95].

As a dark gravity candidate, Finsler geometry has an important scientific potential yet to be explored, despite the fact that it has already been considered in various contexts as an important alternative to Riemann geometry, and the standard ΛCDM paradigm.

Randers geometry was extensively applied in the study of the gravitational phenomena in [96–116]. In [100], generalized Friedmann equations in a Randers–Finsler geometry of the form

$$\dot{H} + H^2 + \frac{3}{4} H Z_t = -\frac{4\pi G}{3}(\rho + 3p), \tag{16}$$

$$\dot{H} + 3H^2 + \frac{11}{4} H Z_t = 4\pi G(\rho - p), \tag{17}$$

were obtained, where H, ρ, and p are the Hubble functions, and the baryonic matter energy density and pressure, respectively. The quantity $Z_t = \dot{u}_0$, with u_0 denoting the time component of the four-velocity u_μ. The generalized Friedmann equations above give the relation $3H^2 + 3HZ_t = 8\pi G\rho$. The term HZ_t, induced by the Finsler–Randers geometry, leads to the existence of new phases in the cosmic evolution of the Universe. The system of Friedmann Equations (16) and (17) was used in [101] for the investigation of particle creation processes in Finsler-type geometries.

A scalar–tensor theory that arises effectively from the Lorentz fiber bundle of a Finsler-type geometry was proposed in [117], where its cosmological implications were also investigated. The action in the presence of matter considered in this work is

$$\mathcal{S} = \frac{1}{16\pi G} \int \sqrt{|\det \mathbf{G}|}\, \mathcal{L}_G dx^{(N)} + \int \sqrt{|\det \mathbf{G}|}\, \mathcal{L}_M dx^{(N)}, \tag{18}$$

where $dx^{(N)} = d^4x \wedge \phi^{(1)} \wedge \phi^{(2)}$. Several Lagrangian densities were adopted, given by

$$\mathcal{L}_G = \tilde{\mathcal{R}} - \frac{1}{\phi} V(\phi), \tag{19}$$

where $V(\phi)$ is the potential for the scalar ϕ, and

$$\tilde{\mathcal{R}} = R - \frac{2}{\phi}\Box\phi + \frac{1}{2\phi^2}\partial_\mu\phi\partial^\mu\phi, \tag{20}$$

where $\Box$ is the d'Alembert operator, and $\tilde{\mathcal{R}}$ denotes the curvature for the particular situation of a holonomic basis $[X_M, X_N] = 0$. In the case of a non-holonomic basis, the adopted Lagrangian density is given by $\overline{\mathcal{L}}_G = \tilde{R}$. The generalized Friedmann equations are given by

$$3H^2 = 8\pi G\rho_m - \frac{\dot{\phi}^2}{4\phi^2} + \frac{1}{\phi}\left(\frac{V(\phi)}{2} - 3H\dot{\phi}\right), \tag{21}$$

$$\dot{H} = -4\pi G(\rho_m + P_m) + \frac{\dot{\phi}^2}{4\phi^2} + \frac{1}{2\phi}(H\dot{\phi} - \ddot{\phi}), \tag{22}$$

$$\ddot{\phi} + 3H\dot{\phi} = -16\pi G\phi\subset_m - 6\phi\left(\dot{H} + 2H^2\right) + \phi V'(\phi) + \frac{\dot{\phi}^2}{2\phi}, \tag{23}$$

and

$$3H^2 = 8\pi G\rho_m - (1+A)\frac{\dot{\phi}^2}{4\phi^2} - 3H\frac{\dot{\phi}}{\phi}, \tag{24}$$

$$\dot{H} = -4\pi G(\rho_m + P_m) + (1+A)\frac{\dot{\phi}^2}{4\phi^2} + \frac{1}{2\phi}(H\dot{\phi} - \ddot{\phi}), \tag{25}$$

$$(1+A)(\ddot{\phi} + 3H\dot{\phi}) = -16\pi G\phi \subset_m - 6\phi\left(\dot{H} + 2H^2\right) + \frac{\dot{\phi}^2}{2\phi}\left(1 + A + \phi A'\right) - \dot{\phi}\dot{A}, \tag{26}$$

respectively. Here, $A(\phi)$ denotes a real function of ϕ. From the above equations, one can reconstruct the thermal history of the Universe, and obtain a sequence of matter and dark-energy-dominated phases. The effective dark energy equation of state has a parameter that can be either phantom or quintessence type. A phantom-divide crossing during the cosmological evolution also appears.

Berwald–Finsler geometries have been investigated as potential candidates for the description of the gravitational fields [118,119]. Spatially homogeneous and isotropic Berwald spacetimes, obtained from a Finsler Lagrangian constructed from a zero-homogeneous function defined on the tangent bundle, and which include the velocity dependence of the Finsler Lagrangian, were discussed in [119]. Cosmological Berwald geometries can also be used for the description of the dynamics of the Universe.

In a series of recent papers [120–123], a systematic investigation of the applications of Finsler geometry in cosmology was considered. The basic geometric ingredients used for the construction of gravitational theories were the (α, β) metrics, and the osculating Barthel connection. One of the basic properties of the Finsler geometry is that an arbitrary point vector field y is associated with each point of the spacetime manifold, with the metric g becoming a function of both x, the coordinates defined on the base manifold, and y, $g = g(x, y)$. In the osculating approach, one assumes the existence of a vector field $Y = Y(x)$, which allows the construction of a Riemannian metric $g(x) = g(x, Y(x))$. In the case of the (α, β) metrics, the connection associated with these metrics, the Barthel connection, is nothing but the Levi–Civita connection associated with $g(x)$.

The introduction of the osculating Barthel connection in the (α, β) spaces of the Finsler geometry leads to a significant simplification of the mathematical formalism, and opens the possibility of constructing unique and well-defined physical models that could be successfully used for the description of the gravitational interaction. In the present review, we briefly introduce, from the perspective of the cosmological applications, the Barthel–Randers, Barthel–Kropina, and conformal Barthel–Kropina models, and we also present their mathematical and theoretical foundations.

From the generalized Friedmann equations of the osculating Barthel–Randers–Kropina cosmological models, obtained by assuming that the background Riemannian metric is of the Friedmann–Lemaitre–Robertson–Walker (FLRW) type, an effective geometric dark energy component can be always generated, which results from the presence of extra terms in the cosmological evolution equations.

A central problem for the physical acceptability of the Finslerian-type models is how successfully they could describe the observational data. The cosmological tests, and comparisons with observational data of these dark energy models, considered in the above-mentioned works are investigated in detail. In the current review, we perform a detailed analysis of the three cosmological models of Barthel–Randers type, introduced in [120], constraining the model parameters. In our investigation, we use 15 Hubble data points (Cosmic Chronometers), the Pantheon Supernovae Type Ia data sample, and the most recent Baryon Acoustic Oscillation (BAO) measurements from the Dark Energy Spectroscopic Instrument (DESI) Data Release 2. The statistical analysis is performed by

using Markov Chain Monte Carlo simulations. The results of the statistical analysis of the Barthel–Randers cosmological models are compared with a similar analysis of the Barthel–Kropina cosmological models performed in [122], and with the standard ΛCDM model. The Akaike information criterion (AIC) and the Bayesian information criterion (BIC) are used as the model selection tools. The statefinder diagnostics, consisting of the study of the jerk and snap parameters, and the $Om(z)$ diagnostics are also considered for the comparative study of the Barthel–Randers, Barthel–Kropina and ΛCDM cosmologies. Our statistical results indicate that the osculating Barthel-type (α, β) Finslerian dark energy models give a good description of the observational data, and thus, they can be considered a viable alternative to the ΛCDM model, even if not all of them are favorable compared to ΛCDM.

The present paper is organized as follows. We review some basic concepts and definitions of Finsler geometry in Section 2. In Section 3, we introduce the mathematical foundations of the Barthel–Randers–Kropina gravitational theories, by reviewing the basic concepts of (α, β) metrics, osculating spaces, and Barthel connections. The basic principles of constructing (α, β) cosmological models are also presented. The generalized Friedmann equations of the three basic models considered in the present work, Barthel–Randers, Barthel–Kropina, and conformal Barthel–Kropina, are also written, together with the corresponding energy balance equations. The thermodynamic interpretation of the cosmological models with a non-vanishing matter energy–momentum tensor is also presented and briefly discussed. The cosmological implications of the Barthel–Randers and Barthel–Kropina models are discussed in Section 4, where constraints on the free parameters of these models are obtained by using a combination of observational datasets, including Type Ia Supernovae, Baryon Acoustic Oscillations, and Hubble parameter measurements. A detailed comparison of the Barthel–Randers and Barthel–Kropina cosmological models is performed in Section 5. A discussion of the main results and the relevance of the statistical analysis is presented in Section 6. Finally, we discuss and conclude our results in Section 7.

2. Fundamentals of Finsler Geometry

The assumption that spacetime can be described mathematically as a four-dimensional differentiable manifold M, endowed with a pseudo-Riemannian tensor g_{IJ}, where $I, J, ... = 0, 1, 2, 3$, is one of the fundamental assumptions of modern theoretical physics. The next fundamental concept, the interval between two events located at the points x^I and $x^I + dx^I$ on the worldline of a standard clock, is defined by the chronological hypothesis as $ds = \left(g_{IJ}dx^I dx^J\right)^{1/2}$ [124,125]. A very important metrical generalization of the Riemannian geometry is the geometry anticipated by Riemann [8], but which was later on systematically developed by Finsler [3].

In a simple interpretation, Finsler spaces are metric spaces with the interval ds between two neighboring points $x = (x^I)$ and $x + dx = (x^I + dx^I)$ given by

$$ds = F(x, dx), \tag{27}$$

where F, the Finsler metric function, must be positively homogeneous of degree one in dx, and thus satisfy the condition

$$F(x, \lambda dx) = \lambda F(x, dx) \quad \text{for} \quad \lambda > 0. \tag{28}$$

The Finsler metric function F can be written in terms of the canonical coordinates of the tangent bundle $(x, y) = (x^I, y^I)$, where $y = y^I(\partial/\partial x^I)$ is any tangent vector y at x. Then we can introduce the Finsler metric tensor g_{IJ} defined according to

$$g_{IJ}(x, y) = \frac{1}{2}\frac{\partial^2 F^2(x, y)}{\partial y^I \partial y^J}. \tag{29}$$

Hence Equation (27) can be written as

$$ds^2 = g_{IJ}(x, y)y^I y^J. \tag{30}$$

Riemann spaces are some particular cases of the Finsler spaces, and they correspond to $g_{IJ}(x, y) = g_{IJ}(x)$ and $y^I = dx^I$, respectively.

Given a Finsler function F, one can obtain the geodesic equations in the form [124,125]

$$\frac{d^2x^I}{d\lambda^2} + 2G^I(x, y) = 0, \tag{31}$$

where the functions $G^I(x, y)$ denote the spray coefficients

$$G^I(x, y) = \frac{1}{4}g^{IJ}\left(\frac{\partial^2 F^2}{\partial x^K \partial y^J}y^K - \frac{\partial F^2}{\partial x^J}\right). \tag{32}$$

Equivalently, more reminiscent of Riemannian geometry, they can be rewritten as

$$\frac{d^2x^I}{d\lambda^2} + \Gamma^I_{JK}(x, y)\frac{dx^J}{d\lambda}\frac{dx^K}{d\lambda} = 0, \tag{33}$$

where

$$\Gamma^I_{JK}(x, y)y^J y^K = 2G^I(x, y) = \frac{1}{2}g^{IJ}\left(\frac{\partial^2 F^2}{\partial x^K \partial y^J}y^K - \frac{\partial F^2}{\partial x^J}\right). \tag{34}$$

Here, the quantities $\Gamma^I_{JK}(x, y)$ are the local coefficients of the Finsler connection used. We point out that the theory of Finsler connections is more complex than in the Riemannian case since the only metrical, torsion-free connection is the Levi–Civita one; hence, the existence of such a connection implies that the Finsler metric is in fact Riemannian. The obvious conditions imposed for the existence of Finsler connections are then non-metricity and torsion-free (this is the case of the Chern connection) or metrical connection with surviving torsion (this is the case of the Cartan connection). The precise form of the Finsler connections depends on the concrete form of the non-metricity and surviving torsion, but these details are beyond the aim of the present paper (one can consult [12,13,126] or other textbooks on Finsler geometry). The local coefficients of a Finsler connection D are defined as

$$D_{\frac{\delta}{\delta x^K}}\frac{\delta}{\delta x^J} = \Gamma^I(x, y)_{JK}\frac{\delta}{\delta x^I}, \quad D_{\frac{\partial}{\partial x^K}}\frac{\partial}{\partial x^J} = V^I(x, y)_{JK}\frac{\partial}{\partial x^I}, \tag{35}$$

where $\frac{\delta}{\delta x^I}$ is the adapted basis induced by the Cartan nonlinear connection. We prefer to keep the notation $C^I_{JK} = \frac{1}{2}\frac{\partial^3 F^2}{\partial y^I \partial y^J \partial y^K}$ for the Cartan tensor of (M, F). For instance, the Cartan connection of a Finsler space (M, F) is the only Finsler connection on TTM that is met-

rical with $h(hh)$ and $v(vv)$-torsion vanishing (the rest of the torsion survives). The local coefficients of the Cartan connection are given by

$$\begin{aligned} \Gamma^I_{JK}(x,y) &= \frac{1}{2}g^{IL}(x,y)\left[\frac{\delta g_{LJ}(x,y)}{\delta x^K}+\frac{\delta g_{LK}(x,y)}{\delta x^J}-\frac{\delta g_{JK}(x,y)}{\delta x^L}\right], \\ V^I_{JK}(x,y) &= \frac{1}{2}g^{IL}(x,y)\left[\frac{\partial g_{LJ}(x,y)}{\partial y^K}+\frac{\partial g_{LK}(x,y)}{\partial y^J}-\frac{\partial g_{JK}(x,y)}{\partial x^L}\right]. \end{aligned} \tag{36}$$

Likewise, the Chern connection is defined to be the only Finsler connection on TTM which is almost compatible and torsion-free. The local coefficients of the Chern connection are given by $(\Gamma^I_{JK}(x,y),0)$. However, despite the rather complicated form of the connection coefficients $\Gamma^I_{JK}(x,y)$, due to the homogeneity of the geometrical objects involved, Equation (33) takes the simple form

$$\frac{d^2x^I}{d\lambda^2}+\gamma^I_{JK}(x,y)\frac{dx^J}{d\lambda}\frac{dx^K}{d\lambda}=0, \tag{37}$$

where

$$\gamma^I_{JK}(x,y)=\frac{1}{2}g^{IL}(x,y)\left[\frac{\partial g_{LJ}(x,y)}{\partial x^K}+\frac{\partial g_{LK}(x,y)}{\partial x^J}-\frac{\partial g_{JK}(x,y)}{\partial x^L}\right], \tag{38}$$

are the formal Christoffel coefficients of the Finsler space (M,F).

Berwald spaces are a special class of Finsler geometry, and they can be obtained by assuming that the Berwald connection coefficients are independent of the fiber coordinate y [10].

With the help of the spray coefficients G^I, one can define the vector field S on $TM\setminus 0$ according to

$$S=y^I\frac{\partial}{\partial x^I}-2G^I\frac{\partial}{\partial y^I}.$$

S is the spray induced by F. A curve γ defined on M is a geodesic of F if and only if its canonical lift $\hat{\gamma}(t)=(\gamma(t),\dot{\gamma}(t))$ to TM is an integral curve of S.

The notion of Finsler metrics that we have recalled here belong to the class of *classic Finsler metrics*; in other words, at each point $x\in M$, the function $F_x: T_xM\to\mathbb{R}$ is a function defined on the tangent space T_xM of a differentiable manifold M satisfying the following conditions:

(i) F_x is C^∞ on $\widetilde{T_xM}=T_xM\setminus\{0\}$.
(ii) F_x is positively 1-homogeneous: $F_x(\lambda y)=\lambda F_x(y)$, for all $\lambda>0$ and $y\in T_xM$.
(iii) For each $x\in M$, the Hessian matrix (29) is positive definite on $\widetilde{T_xM}$.

At each point $x\in M$, the indicatrix $\{y\in T_xM: F_x(y)=1\}$ is a closed, strictly convex, smooth hypersurface around the origin of T_xM.

A more general notion is the notion of conic Finsler metrics, that is, Finsler norms defined only on a conic domain of T_xM. Let us recall that $A_x\subset T_xM$ is called a conic domain of T_xM if A_x is an open, non-empty subset of T_xM such that if $v\in A_x$, then $\lambda v\in A_x$, for all $\lambda>0$. We remark that the origin of T_xM does not belong to A_x except for the case $A_x=T_xM$.

We can now define a Finsler norm defined only on a conic domain $A_x\subset T_xM$ with the properties (i)–(iii) given above for all $y\in A_x$. At each point $x\in M$, the indicatrix $S_x:=\{y\in A_x\subset T_xM: F_x(y)=1\}$ is a hypersurface embedded in A_x as a closed subset.

Let $A \subset TM$ be an open subset of the tangent bundle $\pi : TM \to M$ such that $\pi(A) = M$, and A is conic in TM; that is, for each $x \in M$, the set $A_x := A \cap T_xM$ is a conic domain in T_xM. A function $F : A \to \mathbb{R}$ is a conic Finsler metric if its restriction $F_x : A_x \to \mathbb{R}$ satisfies the conditions (i)–(iii) above, for each $x \in M$. The local and global geometry of conic Finsler spaces can be now developed in a similar way with the case of classical Finsler metrics (see [127,128] and references therein).

3. Osculating (α, β)-Type Cosmological Models

In the present section, we review the mathematical and theoretical foundations of the Barthel–Randers–Kropina-type cosmological models, which we will discuss in the framework of the general (α, β) geometries. We also write down the generalized Friedmann equations obtained for the case of the Friedmann–Lemaitre–Robertson–Walker Riemannian metric. The thermodynamic interpretation of the models is also discussed.

3.1. Mathematical Foundations of the (α, β) Finslerian Cosmologies

We begin our discussion of the cosmology of the Finslerian-type geometries with a brief discussion of the mathematical properties of the (α, β) metrics, the Barthel connection, and the osculating geometries.

3.1.1. Kropina and (α, β) Geometries

As we have already mentioned, a special type of Finsler space is the Randers space [25], with the metric function given by

$$F = \left[a_{IJ}(x)y^I y^J\right]^{1/2} + b_I(x)y^I, \tag{39}$$

where a_{IJ} is the metric tensor of a Riemannian space, and $b_I(x)y^I$ is a linear 1-form defined on the tangent bundle TM, and we use the parametrization $dx^I = y^I$.

Another remarkable class of Finsler spaces are the Kropina spaces [129,130], which are Finsler spaces with metrics of the form

$$F(x, y) = \frac{a_{IJ}(x)y^I y^J}{b_I(x)y^I}. \tag{40}$$

By generalizing these results, Matsumoto [131,132] defined the notion of the (α, β) metrics in the following way: given a Finsler metric function $F(x, y)$, it is called an (α, β) metric if F is a positively homogeneous function $F(\alpha, \beta)$ of first degree in two variables $\alpha(x, y) = \left[a_{IJ}(x)y^I y^J\right]^{1/2}$ and $\beta(x, y) = b_I(x)y^I$, respectively.

In our analysis, we suppose that α is a pseudo-Riemannian or Riemannian metric, with the properties that it is non-degenerate (regular), or positive definite. We point out that the Kropina-type metrics are conic Finsler metrics defined only on some conic domain of the tangent bundle. By extension, we can regard any (α, β) as conic Finsler metrics, allowing the Riemannian part to be a pseudo-Riemannian metric.

In the special cases of the Randers and Kropina metrics, the Finsler metric functions are given by $F = \alpha + \beta$, and $F = \frac{\alpha^2}{\beta}$, respectively (see also Table 1). Therefore the Randers and Kropina metrics belong to the general class of the (α, β) metrics.

We can define the general (α, β) metrics as metrics having the metric function given by

$$F(\alpha, \beta) = \alpha\phi(\beta/\alpha) = \alpha\phi(s), \tag{41}$$

where $s = \beta/\alpha$, and $\phi = \phi(s)$ is a C^∞ positive function on an open interval $(-b_o, b_o)$.

Many examples of (α, β) metrics have been considered in the literature, the most studied one being the Randers metric $F = \alpha + \beta$ (see [133] and references within). The Kropina metrics are also classic examples of (α, β) metrics (see [134] for physical motivations of introducing this metric). More recently, the local and global aspects of Kropina metrics have been extensively studied in [128,135–138].

3.1.2. The Barthel Connection

Let (M^n, F) be a Finsler space, defined on a base manifold M^n. We can also define on M^n a vector field $Y(x) \neq 0$. We introduce now a specific mathematical object $(M^n, F(x,y), Y(x))$, which represents a Finsler space $(M^n, F(x,y))$ with a tangent vector field $Y(x)$ also defined. If the vector Y does not vanish at any point on M, then from the Finslerian metric $\widehat{g}(x,y)$, one obtains the Y-Riemann metric $\widehat{g}_Y(x) = \widehat{g}(x,Y)$.

Obviously, one can evaluate any geometrical object in a Finsler space (M,F) in the specific direction given by a fixed vector field Y. This remark leads to the natural idea of evaluating the Chern connection coefficients $\Gamma^I_{JK}(x,y)$ given in (36) at $y = Y(x)$. This is the so-called Barthel connection introduced by Barthel himself in [139,140] and developed later by Ingarden and Matsumoto [134].

The Barthel connection is an affine connection on $(M, \widehat{g}_Y)$, metrical with torsion

$$T^I_{JK}(x) = V^I_{LJ}(x, Y(x))Y^L_K - V^I_{LK}(x, Y(x))Y^L_J, \tag{42}$$

where $Y^L_J(x) := \frac{\partial Y^L}{\partial x^J} - N^L_J(x, Y(x))$ and $N^L_J(x,y)$ is the Cartan nonlinear connection of the Finsler space (M,F).

The local coefficients of the Barthel connection can be written as

$$b^I_{JK}(x) = F^I_{JK}(x, Y(x)) + V^I_{JL}(x, Y(x))Y^L_J(x). \tag{43}$$

The absolute differential of the vector Y is defined according to [141]

$$DY^I = dY^I + Y^K b^I_{KH}(x,Y)dx^H, \tag{44}$$

where by $b^I_{KH}(x,Y)$ we have denoted the coefficients of the Barthel connection. By using the homogeneity of the geometrical objects involved, we obtain

$$DY^I = dY^I + Y^K\left(\widehat{\gamma}^I_{KH} - \widehat{\gamma}^R_{KS}Y^S\widehat{C}^I_{RH}\right)dx^H. \tag{45}$$

The Barthel connection has a number of interesting properties. It depends on the vector field on which it acts, a property that does not exist in Riemann geometry. Therefore, the Barthel connection has very different properties, and so it significantly differs from the connections in Riemann geometry. Another important property is related to the direction and magnitude dependence of the Barthel connection. For anisotropic metrics, like most of the Finsler metrics, all geometric properties depend on the direction. For the Barthel connection, there is no dependence on the magnitude of the vector field, but only on its direction. The Barthel connection, keeping the metric function unchanged by the parallel transport, is the simplest connection with this property. For Finsler vector fields, depending on both x and y, the Barthel connection allows the transition to the Cartan geometry of the Finsler spaces. Moreover, the Barthel connection can be considered as the connection of a point in Finsler space.

Finally, we would like to mention that unlike the Levi–Civita connection of the Riemannian geometry, the Finsler connections (Cartan or Chern connections) are not defined on the base manifold M, but they live on the total space of the tangent bundle [12,13]. On the other

hand, even though they are completely different, the Barthel and Levi–Civita connections are affine connections on the base manifold M. This is a very important characteristic of Barthel-type geometries that leads to significant differences between the geometrical theories of gravity as formulated on Riemann and Finsler manifolds.

3.1.3. The Y-Osculating Riemann Geometry

In 1936, Nazim [142] introduced and developed the concept of osculating Riemann spaces of Finsler geometries. This concept was later studied by Varga [143]. In the osculating approach, one associates to a complex geometric object, like a Finsler geometry and connection, a simpler mathematical structure, for example, an affine or a linear connection, or a Riemann metric. Hence, in this approach, it is assumed that the osculating geometry approximates the more complicated one at a certain level. Thus, with the use of the osculating formalism, one can derive mathematical results that significantly simplify the description of the properties of the mathematically complex geometries.

Let a nowhere-vanishing local section Y of $\pi_M : TM \to M$ be given. Geometric objects existing on TM can be pulled back to M. Since $g_{IJ} \circ Y$ is a function defined on U, a new metric, defined according to

$$\widehat{g}_{IJ}(x) := g_{IJ}(x,y)|_{y=Y(x)}, \quad x \in U, \tag{46}$$

can be introduced. The pair $(U, \widehat{g}_{IJ})$ represents a Riemannian manifold, while $\widehat{g}_{IJ}(x)$ is the Y- osculating Riemannian metric, defined on (M, F).

For the osculating Riemannian metric given by Equation (46), we define the Christoffel symbols of the first kind as

$$\widehat{\gamma}_{IJK}(x) := \frac{1}{2}\left\{\frac{\partial}{\partial x^J}[g_{IK}(x,Y(x))] + \frac{\partial}{\partial x^K}[g_{IJ}(x,Y(x))] - \frac{\partial}{\partial x^I}[g_{JK}(x,Y(X))]\right\}. \tag{47}$$

With the use of the rule of the derivative of the composed functions, we explicitly find

$$\widehat{\gamma}_{IJK}(x) = \gamma_{IJK}(x,y)\big|_{y=Y(x)} + 2\left(C_{IJL}\frac{\partial Y^L}{\partial x^K} + C_{IKL}\frac{\partial Y^L}{\partial x^J} - C_{JKL}\frac{\partial Y^L}{\partial x^I}\right)\Big|_{y=Y(x)}, \tag{48}$$

where C_{IJL} denotes the Cartan tensor. Hence, if a global section Y of TM exists, so that $Y(x) \neq 0, \forall x \in M$, one can always define the osculating Riemannian manifold $(M, \widehat{g}_{ij})$.

The case of the (α, β) metrics.

Let us focus now on the case of the (α, β) metrics. The Hessian matrix of an (α, β)-metric $F = F(\alpha, \beta)$ is given by

$$g_{IJ}(x,y) = \frac{L_\alpha}{\alpha}h_{IJ} + \frac{\partial L_{\alpha\alpha}}{\alpha^2}y_I y_J + \frac{\partial L_{\alpha\beta}}{\alpha}(y_I b_J + y_J b_i) + L_{\beta\beta}b_I b_J, \tag{49}$$

and the Cartan tensor by

$$2C_{IJK} = \frac{L_{\alpha\beta}}{\alpha}(h_{IJ}p_K + h_{JK}p_I + h_{KI}p_J) + L_{\beta\beta\beta}p_I p_J p_K, \tag{50}$$

where the notation $L := \frac{F^2}{2}$ is customary. Here, $p_I = b_I - \frac{\beta}{\alpha}y_I$, and $h_{IJ} = g_{IJ} - \frac{y_I y_J}{F^2}$ is the angular tensor of (M, F).

We choose the vector field as $Y = b$, with $b^I = a^{IJ}b_J$. Since the vector field Y is globally non-vanishing on M, we obtain the result that β has no zero points on M. Hence, we

can define for the (α, β) metrics the b- osculating Riemannian manifold $(M, \widehat{g}_{IJ})$, with the Riemannian metric given by $\widehat{g}_{IJ}(x) := g_{IJ}(x, b)$, where $b^I = a^{IJ}b_J$.

With respect to α, the length $\widetilde{b}$ of b is obtained as $\widetilde{b}^2 = b_I b^I = \alpha^2(x, b)$. Moreover, we have $Y_I(x, b) = b_I$, respectively.

The b-osculating Riemannian metric can be explicitly written as

$$\widehat{g}_{IJ}(x) = \frac{L_\alpha}{\widetilde{b}}\bigg|_{y=b(x)} g_{IJ} + \left(\frac{L_{\alpha\alpha}}{\widetilde{b}^2} + 2\frac{L_{\alpha\beta}}{\widetilde{b}} + L_{\beta\beta} - \frac{L_\alpha}{\widetilde{b}^3}\right)\bigg|_{y=b(x)} b_I b_J. \tag{51}$$

Moreover, we obtain $\beta(x, b) = \widetilde{b}^2$, and $p_I(x, b) = 0$. Hence, by using the expression of the Cartan tensor for an (α, β) metric, we obtain the important result that $C_{IJK}(x, b) = 0$. For $Y = b$, we find

$$\widehat{\gamma}_{IJK}(x) = \gamma_{IJK}(x, y)\big|_{y=b(x)}. \tag{52}$$

Thus, we have obtained the fundamental result that in the case of an (α, β)-metric, the Barthel connection, representing the linear b-connection, where $b^I = \left(a^{IJ}b_J\right)$, is the Levi–Civita connection of the b-Riemannian metric. Hence, after the evaluation of the fundamental Finsler tensor $g_{ij}(x, y)$ of (M, F) at the point $(x, Y(x))$, we obtain a Riemannian metric $\widehat{g}_Y$ on M, with its Levi–Civita connection.

The curvature tensor.

The Barthel connection with local coefficients $\left(b^A_{BC}(x)\right)$ is an affine connection. We define the curvature tensor of an affine connection, having local coefficients $\left(\Gamma^A_{BC}(x)\right)$, as

$$R^A_{BCD} = \frac{\partial \Gamma^A_{BD}}{\partial x^C} - \frac{\partial \Gamma^A_{BC}}{\partial x^D} + \Gamma^E_{BD}\Gamma^A_{EC} - \Gamma^E_{BC}\Gamma^A_{ED}. \tag{53}$$

Thus, it follows that the curvature of the Barthel connection can be obtained from Equation (53) by taking $\left(\Gamma^A_{BC}(x)\right) = \left(b^A_{BC}(x)\right)$. For the Kropina metric with $F = \alpha^2/\beta$, the Barthel connection is equal to the Levi–Civita connection of the osculating metric $\widehat{g}_{AB}(x) = g_{AB}(x, b(x))$, with $b_I(x)$ denoting the components of the one-form β. Moreover, g_{AB} is the fundamental tensor of F.

Since $b^A_{BC} = \widehat{\gamma}^A_{BC}$, where $\widehat{\gamma}^A_{BC}$ are the coefficients of the Levi–Civita connection, for the curvature tensors of the Kropina metric, we find the expressions

$$\widehat{R}^A_{BCD} = \frac{\partial \widehat{\gamma}^A_{BD}}{\partial x^C} - \frac{\partial \widehat{\gamma}^A_{BC}}{\partial x^D} + \widehat{\gamma}^E_{BD}\widehat{\gamma}^A_{EC} - \widehat{\gamma}^E_{BC}\widehat{\gamma}^A_{ED}, \tag{54}$$

and

$$\widehat{R}_{BD} = \sum_A \left[\frac{\partial \widehat{\gamma}^A_{BD}}{\partial x^A} - \frac{\partial \widehat{\gamma}^A_{BA}}{\partial x^D} + \sum_E \left(\widehat{\gamma}^E_{BD}\widehat{\gamma}^A_{EA} - \widehat{\gamma}^E_{BA}\widehat{\gamma}^A_{ED}\right)\right], \tag{55}$$

respectively, where the indices A, B, C, D, E take the values $\{0, 1, 2, 3\}$, and we have defined $\widehat{R}_{BD} = \widehat{R}^A_{BAD}$, and $\widehat{R}^B_D = \hat{g}^{BC}\widehat{R}_{CD}$, respectively [120–123]. The generalized Ricci scalar is defined according to $\widehat{R} = \widehat{R}^B_B$.

3.2. Building Cosmological Models in (α, β) Geometries

We proceed now to the investigation of the possibility of using the Finslerian geometric framework, and the general (α, β) metrics, to build specific cosmological models. Our basic quantities in this respect are the Riemannian metric a_{IJ}, which determines $\alpha = a_{IJ}dx^I dx^J = a_{IJ}y^I y^J$, and the coefficient b_I of the one-form $\beta = b_I dx^I = b_I y^I$. To construct a cosmological model in the (α, β)-type Finsler geometries, we introduce several assumptions, detailed below.

The Universe is homogeneous and isotropic.

As a first approximation of the structure and matter distribution in the Universe, we assume the validity of the cosmological principle. The cosmological principle implies the homogeneity of the Universe. The homogeneity of the Universe imposes the fundamental constraint that on large cosmological scales, all the physical and geometrical properties of the Universe depend globally on the cosmological time only.

The Riemannian metric a_{IJ} is the FLRW metric.

In the following, we will restrict our study to the case in which the metric a in the definition of $\alpha = a_{IJ}dx^I dx^J$ is the flat, homogeneous and isotropic Friedmann–Lemaitre–Robertson–Walker (FLRW) metric. In a system of coordinates $\left(x^0 = ct, x^1 = x, x^2 = y, x^3 = z\right)$ defined on the base manifold M, the Riemannian FLRW metric is given by

$$ds_R^2 = g_{IJ}dx^I dx^J = c^2dt^2 - a^2\left(x^0\right)\left(dx^2 + dy^2 + dz^2\right), \tag{56}$$

where t is the universal cosmological time, c is the speed of light, and $a\left(x^0\right)$ is the scale factor, describing the expansionary properties of the Universe. From an observational point of view, the Hubble function, defined as $H = \left(1/a\left(x^0\right)\right)\left(da\left(x^0\right)/dx^0\right)$, plays an important role, since it allows the in depth comparison of the astrophysical data with the theoretical predictions.

The Finsler metric depends on x^0 only.

The cosmological principle, together with the homogeneity postulates, requires that together with $a_{IJ} = a_{IJ}\left(x^0\right)$, the components of the 1-form β are also functions of the cosmological time only, $b_I = b_I\left(x^0\right)$.

The 1-form b has vanishing space-like components.

The cosmological principle, requiring the homogeneity of the Universe, as well as the isotropy condition that follows from the choice of the Riemann metric as the FLRW metric, with only diagonal components, leads to a strong mathematical constraint on the components of the coefficients of the 1-form b. The isotropy of the metric imposes the condition that all the space-like components of A identically vanish, so that $b_1 = b_2 = b_3 = 0$. If this restriction is not satisfied, then after performing a spatial rotation in the (x, y, z) three-dimensional space, we can construct a preferred direction, oriented, for example, in the direction of the x coordinate. But the possibility of such a transformation and the existence of a preferred direction would contradict the isotropic condition implemented via the FLRW metric, as well as the observed large-scale spatial isotropy of the Universe. Hence, in the present approach to Finslerian cosmology, we assume that the vector b has only one independent component, so that $b_0\left(x^0\right)$. Therefore, in a homogeneous and isotropic cosmology, the 1-form field b takes the simple form

$$\left(b_I\right) = \left(a\left(x^0\right)\eta\left(x^0\right), 0, 0, 0\right) = \left(b^I\right), \tag{57}$$

where we have introduced the auxiliary function $\eta\left(x^0\right)$ to obtain a representation of b_0 in terms of the scale factor of the Universe.

Matter moves along the Hubble flow.

We assume that similarly to the standard general relativistic cosmology, defined in the Riemannian geometric setting, in Finslerian cosmology, we can also introduce a comoving frame in which the cosmological observers, as well as ordinary matter, move along with the Hubble flow, defined by the metric $a_{IJ}(x)$. If we introduce the Riemannian

four-velocities u^I of the matter particles, defined as $u^I = dx^I/ds_R$, then the existence of a moving frame implies that the space-like components of the matter four-velocity vanish identically, and the four-velocity has only a non-zero temporal component $u^I = (1, 0, 0, 0)$, which can be normalized to one.

The matter content of the Universe is a perfect fluid.

We postulate that cosmological matter in the Universe consists of a perfect fluid, whose thermodynamic properties can be described by two basic thermodynamic quantities only, given by the energy density ρc^2, and the thermodynamic pressure p, respectively. We also assume that the thermodynamic quantities can be defined in the usual way, by using the standard definitions of statistical physics and thermodynamics. From assumptions *c* and *d* it follows that the matter energy–momentum tensor has only two non-zero components, $\widehat{T}^0_0 = \rho c^2$, and $\widehat{T}^I_I = -p$, $I = 1, 2, 3$, and thus, it can be represented in the form

$$\widehat{T}^J_I = \begin{pmatrix} \rho c^2 & 0 & 0 & 0 \\ 0 & -p & 0 & 0 \\ 0 & 0 & -p & 0 \\ 0 & 0 & 0 & -p \end{pmatrix}. \tag{58}$$

Geometric quantities.

Once the above conditions and assumption have been adopted, we obtain the expressions of the Finsler metric, and of α and β in the FLRW cosmological background of the osculating Barthel–(α, β) geometry as follows:

(iii) $$(a_{IJ}) = \begin{pmatrix} 1 & 0 & 0 & 0 \\ 0 & -a^2(x^0) & 0 & 0 \\ 0 & 0 & -a^2(x^0) & 0 \\ 0 & 0 & 0 & -a^2(x^0) \end{pmatrix};$$

(iv) $$\alpha|_{y=b(x)} = a(x^0)\eta(x^0);$$

(v) $$\beta|_{y=b(x)} = [a(x^0)\eta(x^0)]^2;$$

(vi) $$(h_{IJ}|_{y=b(x)}) = \begin{pmatrix} 0 & 0 & 0 & 0 \\ 0 & -a^2(x^0) & 0 & 0 \\ 0 & 0 & -a^2(x^0) & 0 \\ 0 & 0 & 0 & -a^2(x^0) \end{pmatrix}.$$

where $I, J \in \{0, 1, 2, 3\}$, and $h_{IJ}(x, y) := a_{IJ} - \frac{y_I}{\alpha}\frac{y_J}{\alpha}$ is the angular metric of (M, α). From the above expressions, it turns out that the Finsler metric g is also diagonal. This result follows in a natural way from the definition of the (α, β) metric. Thus, in this Finslerian modification of general relativity, we maintain one of the essential properties of the FLRW metric (56), namely homogeneity and isotropy of the Riemannian geometry.

Gravitational field equations.

We postulate that the Einstein gravitational field equations, which geometrically describe the properties of the gravitational interaction, can be formulated in a general (α, β) Finslerian geometry as

$$\widehat{G}_{IJ} = \widehat{R}_{IJ} - \frac{1}{2}\widehat{g}_{IJ}\widehat{R} = \frac{8\pi G}{c^4}\widehat{T}_{IJ}, \tag{59}$$

where G is the gravitational constant. These equations are the natural extension of the Riemannian Einstein equations in the Finslerian framework. They reduce to the standard general relativistic Einstein equations in the limiting case of the Riemann geometry.

Flowchart of the algorithmic construction of osculating Barthel-type Finslerian gravitational theories.

The steps necessary to construct a specific Barthel–Kropina-type cosmological model, and the underlying gravitational theory, are presented algorithmically in the form of a flowchart in Figure 1.

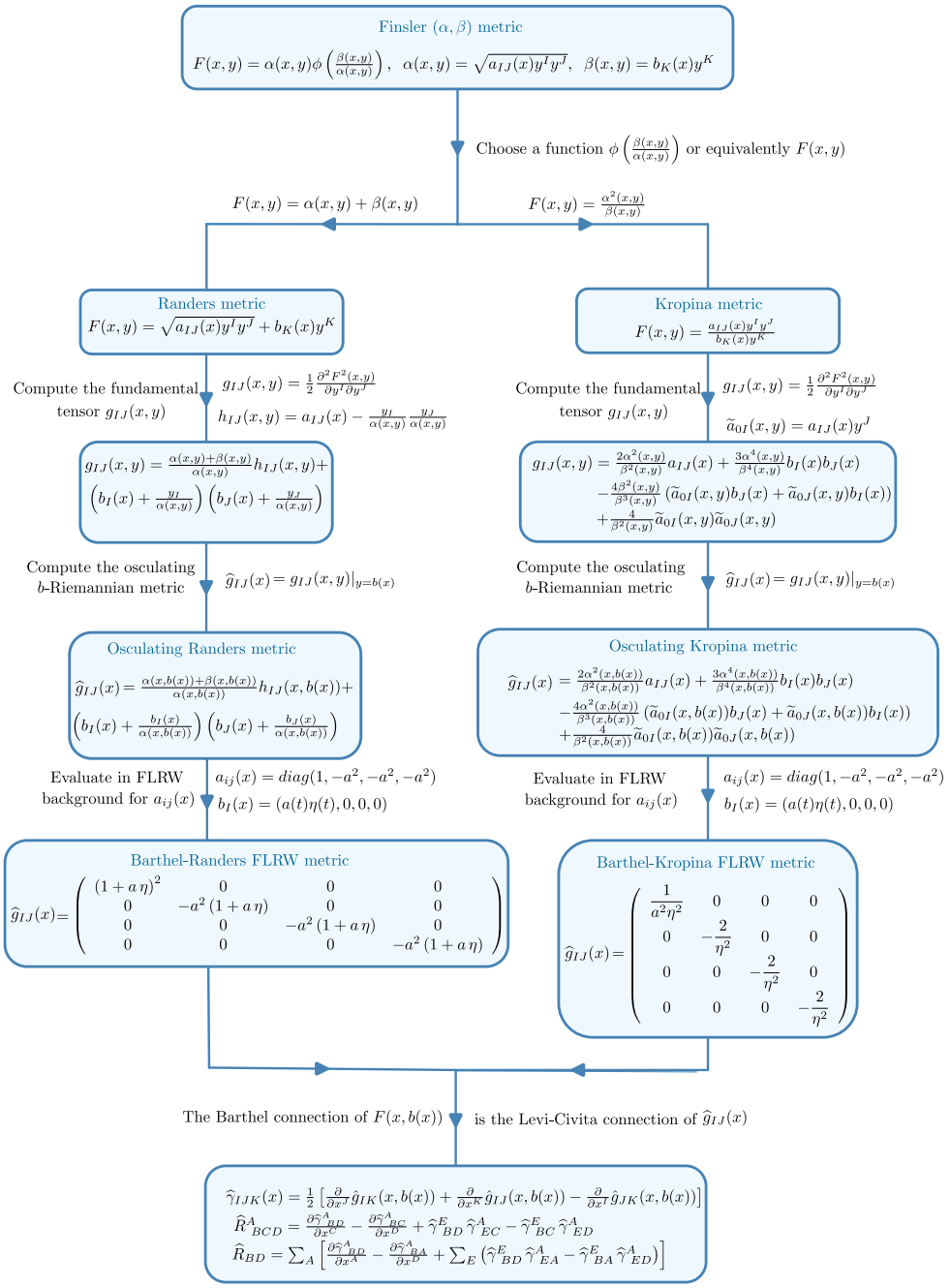


Figure 1. Flowchart of the algorithmic approach for the construction of the (α,β) gravitational models with the Barthel connection.

Although specific examples are restricted to the cases of Barthel–Randers and Barthel–Kropina geometries, the formalism can be easily extended to any other choices of the Finslerian function $F=\alpha\phi(s)$, and the implementation of the geometrical model into a gravitational theoretical framework can be performed easily. In all these cases, some

extensions of standard general relativity can be obtained, leading to gravitational field equations that contain extra Finslerian terms, which in a cosmological context can be interpreted as describing an effective geometric dark energy, generated by the nonlocal geometric structure of the spacetime, with the metric tensor nonlocalized due to the presence of the vector y, representing an internal degree of freedom.

There are a large number of (α, β) metrics, whose physical and gravitational properties are worth investigating, and which could offer new and important insights into the gravitational and cosmological phenomena. The flowchart of the algorithmic approach presented in Figure 1 may simplify and clarify the necessary steps taken for the investigation of these classes of theories.

3.3. Barthel–Randers Cosmology

For the case of the Randers geometry, we have $F = \alpha + \beta$. By using the above assumptions, it turns out that the generalized Friedmann equations in this geometry take the form [120]

$$3H^2 = 8\pi G\phi^2\rho - \frac{3}{4}\frac{\dot{\phi}^2}{\phi^2} - 3H\frac{\dot{\phi}}{\phi}, \tag{60}$$

and

$$2\dot{H} + 3H^2 = -\frac{8\pi G}{c^2}\phi^2 p - \frac{\ddot{\phi}}{\phi} + \frac{5}{4}\frac{\dot{\phi}^2}{\phi^2} - H\frac{\dot{\phi}}{\phi}, \tag{61}$$

where we have denoted

$$\phi\left(x^0\right) = 1 + a\left(x^0\right)\eta\left(x^0\right). \tag{62}$$

Equations (60) and (61) give the dynamical evolution of H as

$$\dot{H} = -4\pi G\phi^2\left(\rho + \frac{p}{c^2}\right) - \frac{\ddot{\phi}}{2\phi} + \frac{\dot{\phi}^2}{\phi^2} + H\frac{\dot{\phi}}{\phi}. \tag{63}$$

Equation (60) can be rewritten as

$$3\left(H + \frac{\dot{\phi}}{2\phi}\right)^2 = 8\pi G\phi^2\rho. \tag{64}$$

By introducing the new Hubble function defined as

$$\widetilde{H} = H + \frac{\dot{\phi}}{2\phi}, \tag{65}$$

we obtain the final form of the generalized Friedmann equations in the Barthel–Randers cosmology as

$$3\widetilde{H}^2 = 8\pi G\phi^2\rho, \tag{66}$$

and

$$2\dot{\widetilde{H}} + 3\widetilde{H}^2 = -\frac{8\pi G}{c^2}\phi^2 p + \frac{\dot{\phi}^2}{\phi^2} + 2H\frac{\dot{\phi}}{\phi}, \tag{67}$$

respectively.

The energy conservation equation.

The energy conservation equation of the matter in the present model of the Barthel–Randers cosmology can be obtained by assuming that similarly to the standard Riemannian general relativistic case, the covariant divergence of the energy–momentum tensor vanishes, $\widehat{\nabla}_\mu T^{\mu\nu} = 0$, with the covariant derivative calculated with the help of the Barthel–Randers

connection $\widehat{\gamma}^{\mu}{}_{\nu\alpha}$. Hence, the conservation equation in Barthel–Randers cosmology can be written as [120]

$$\dot{\rho} + 3\left(H + \frac{\dot{\phi}}{2\phi}\right)\left(\rho + \frac{p}{c^2}\right) = 0, \tag{68}$$

or, in an alternative form, as

$$\frac{d}{dt}\left(\rho a^3\right) + \frac{p}{c^2}\frac{d}{dt}a^3 + \frac{3}{2}a^3\left(\rho + \frac{p}{c^2}\right) = 0. \tag{69}$$

The conservation equation is not independent, and can be also derived directly with the use of the Friedman equations. By taking the time derivative of Equation (60), and after substituting $\dot{H}$ from Equation (61), we find

$$\begin{aligned} &8\pi G\phi^2\left(\dot{\rho} + \frac{3Hp}{c^2}\right) - \frac{3}{8\phi^3}(\dot{\phi}^3 - 2H\phi\dot{\phi}^2 - 20H^2\phi^2\dot{\phi}^2) \\ &+ 4\pi G\phi\dot{\phi}(3p + 4\rho) + 9H^3 = 0. \end{aligned} \tag{70}$$

By substituting the expression of H^2 from the Friedmann Equation (60), we recover Equation (70).

3.4. Barthel–Kropina Cosmology

In the Kropina geometry, the Finslerian metric function is given by $F = \alpha^2/\beta$. The generalized Friedmann equations can be obtained directly from the Einstein equations, and are given by [121]

$$\frac{3(\eta')^2}{\eta^2} = \frac{8\pi G}{c^2}\frac{1}{a^2\eta^2}\rho, \tag{71}$$

and

$$2\frac{\eta''}{\eta} + 2\mathcal{H}\frac{\eta'}{\eta} - 3\frac{(\eta')^2}{\eta^2} = \frac{8\pi G}{c^4}\frac{p}{a^2\eta^2}, \tag{72}$$

respectively, where $\mathcal{H}$ denotes the generalized Hubble function of the Barthel–Kropina cosmology, defined according to $\mathcal{H} = \left(1/a\left(x^0\right)\right)\left(da\left(x^0\right)/dx^0\right)$.

In the above equations, and in the following, a prime denotes the derivative with respect to x^0, a dot denotes the derivative with respect to the cosmological time t, and the standard Hubble function is given by $H = c\mathcal{H}$. After eliminating the term $-3(\eta')^2$ with the help of Equations (71) and (72), it becomes [121]

$$a\eta\frac{d}{dx^0}(\eta' a) = \frac{4\pi G}{c^4}\left(\rho c^2 + p\right). \tag{73}$$

In the Barthel–Kropina geometry, the full system of the generalized Friedmann equations is represented by two ordinary differential equations with four unknowns (a, η, ρ, p). By considering an equation of state for the baryonic matter, $p = p(\rho)$, the number of unknowns in the system of generalized Friedmann equations becomes three, and the system is still underdetermined. Therefore, to obtain solvable cosmological models, and to close the system, we must impose a supplementary independent relation on two of the model parameters.

Energy balance equation.

One of the basic consequences of the standard Friedmann cosmology is the conservation of the matter energy–momentum tensor. But as one can easily observe from the Friedmann Equations (71) and (72), this property does not hold anymore in the Barthel–Kropina cosmology. The matter non-conservation equation as well as the energy density balance equation can be obtained after the multiplication of Equation (71) with a^3, and applying the time derivation operator d/dx^0 on the result. By using the second generalized

Friedmann equation in the obtained relation, the energy non-conservation equation in the Barthel–Kropina cosmology is obtained as [121]

$$\frac{8\pi G}{c^4}\left[\frac{d}{dx^0}\left(\rho c^2 a^3\right)+p\frac{d}{dx^0}a^3\right]=6a^5\left[\mathcal{H}(\eta')^2+(\eta'+\mathcal{H}\eta)\eta''+\mathcal{H}^2\eta\eta'\right]. \tag{74}$$

Equation (74) can be written in a form similar to the standard general relativistic conservation equation as

$$\frac{4\pi G}{c^4}\left[\frac{d}{dx^0}\left(\rho c^2 a^3\right)+p\frac{d}{dx^0}a^3\right]=3a^5\left[\frac{8\pi G}{2c^4}\left(\frac{5}{3}\rho c^2+p\right)\frac{\mathcal{H}}{a^2}+\eta'\eta''\right]. \tag{75}$$

The general relativistic limit.

An interesting and important property of the generalized Friedmann equations of the Barthel–Kropina cosmological model, given by Equations (71) and (72), is that they admit a general relativistic limit, in which they take the form of the standard Friedmann equations of general relativity. The general relativistic limit is given by [121]

$$\eta\to\pm\frac{1}{a},\beta\to(1,0,0,0). \tag{76}$$

Then from Equations (71) and (72), we immediately reobtain the Friedmann equations of standard general relativity

$$\frac{3(a')^2}{a^2}=\frac{8\pi G}{c^2}\rho,\ \ 2\frac{a''}{a}+\frac{(a')^2}{a^2}=-\frac{8\pi G}{c^4}p. \tag{77}$$

From Equation (77), it follows that the energy density ρ is conserved, with the conservation equation given by $\dot{\rho}+3H\left(\rho+p/c^2\right)=0$.

3.5. Conformal Barthel–Kropina Cosmology

Let us consider that an (α,β)-metric with $F=F(\alpha,\beta)$ is given. The conformal transformation of the metric is defined as [123]

$$\widetilde{F}(x,y):=e^{\sigma(x)}F(x,y)=\widetilde{F}\left(\widetilde{\alpha},\widetilde{\beta}\right). \tag{78}$$

The metric (78) is again an $\left(\widetilde{\alpha},\widetilde{\beta}\right)$ metric, with

$$\widetilde{\alpha}=e^{\sigma(x)}\alpha,\ \widetilde{\beta}=e^{\sigma(x)}\beta. \tag{79}$$

The fundamental tensor of $\widetilde{F}$ is calculated with the help of the Hessian [123]

$$\widetilde{g}_{IJ}:=\frac{1}{2}\frac{\partial^2\widetilde{F}^2}{\partial y^I\partial y^J}. \tag{80}$$

The conformal transformation of the Kropina metric is obtained as

$$\widetilde{F}:=e^{\sigma(x)}\frac{\alpha^2}{\beta}=\frac{\widetilde{\alpha}^2}{\widetilde{\beta}},$$

where $\widetilde{\alpha}=e^{\sigma(x)}\alpha$, $\widetilde{\beta}=e^{\sigma(x)}\beta$. The osculating Riemannian metric is obtained as

$$\widehat{\widetilde{g}}_{IJ}(x)=e^{2\sigma(x)}\widehat{g}_{IJ}(x), \tag{81}$$

where $\widehat{g}_{IJ}(x)$ is given by

$$\widehat{g}_{IJ}(x, b(x)) = \frac{2\alpha^2}{\beta^2} a_{IJ}(x) + \frac{3\alpha^4}{\beta^4} b_I b_J - \frac{4\alpha^2}{\beta^3}(b_I b_J + b_J b_I) + \frac{4}{\beta^2} b_I b_J, \tag{82}$$

where $b_I := a_{IJ} b^J = \widetilde{a}_{0I}(x, b(x))$ (see Figure 1). For cosmological applications we choose the conformal factor as $\sigma(x) = \phi(x^0)$. Hence in the study of the dynamical evolution of the Universe, we will restrict our investigations to conformal transformations of the Kropina metric that depend only on time.

The generalized Friedmann equations.

In the conformal Barthel–Kropina geometry, the generalized Friedmann equations take the form [123]

$$\frac{3(\eta')^2}{\eta^2} = \frac{8\pi G}{c^2} \frac{1}{a^2\eta^2} \widetilde{\rho} + 3(\phi')^2 - 6\frac{\eta'}{\eta}\phi', \tag{83}$$

and

$$\frac{2}{\eta^2}[-3(\eta')^2 + 2\eta\eta'\mathcal{H} + 2\eta\eta''] = \frac{16\pi G}{c^4} \frac{1}{a^2\eta^2} \widetilde{p} - 4\left[\phi'' + \frac{1}{2}(\phi')^2\right] + \left(\frac{\eta'}{\eta} - \mathcal{H}\right)\phi', \tag{84}$$

respectively. We eliminate now the term $-3(\eta')^2/\eta^2$ between Equations (83) and (84), and thus we find the relation

$$2\frac{1}{a\eta}\frac{d}{dx^0}(a\eta') = \frac{4\pi G}{c^4} \frac{1}{a^2\eta^2}\left(\widetilde{\rho}c^2 + \widetilde{p}\right) - \left(\phi'' - (\phi')^2\right) - \frac{11}{4}\frac{\eta'}{\eta}\phi' - \frac{1}{4}\phi'\mathcal{H}. \tag{85}$$

The general relativistic limit of the system (83) and (84) is obtained by taking $\eta \to 1/a$, and $(b_I(x)) = (1, 0, 0, 0)$, respectively. Consequently, $\beta = y^0$. Thus, in this limit, the generalized Friedmann cosmological evolution equations of the conformal Barthel–Kropina model become [123]

$$3\mathcal{H}^2 = \frac{8\pi G}{c^4}\widetilde{\rho}c^2 + 3(\phi')^2 + 6\mathcal{H}\phi', \tag{86}$$

and

$$2\mathcal{H}' + 3\mathcal{H}^2 = -\frac{8\pi G}{c^4}\widetilde{p} + 2\left[\phi'' + \frac{1}{2}(\phi')^2\right] + \mathcal{H}\phi', \tag{87}$$

respectively. For $\phi = 0$ we fully recover the standard Friedmann equations of general relativity.

3.6. Thermodynamic Interpretation of the (α, β) Cosmologies

It is a general property of several Finslerian-type cosmological models that the matter energy–momentum is not conserved. For example, Equation (68) illustrates this situation for the case of the Barthel–Randers cosmological models. Hence, contrary to the general relativistic case, in the Barthel–Randers-type cosmological model, as well as in the Barthel–Kropina and conformally transformed Barthel–Kropina cosmologies, the baryonic matter content of the Universe is not conserved anymore. This intriguing property of the models raises the problem of the physical interpretation of the non-conservation of the matter energy–momentum tensor, and the problem of the cosmological significance of this effect.

A possible physical understanding of the energy–momentum non-conservation can be obtained by interpreting this effect by using the thermodynamics of irreversible processes, and assuming that it describes particle creation and annihilation in a cosmological environment. In the following, we briefly introduce first the foundations of the thermodynamics

of irreversible processes, and then we illustrate the general formalism by considering the specific case of the Barthel–Randers-type cosmological model. The non-conservation of the energy–momentum tensor is a specific feature of several modified gravity theories, and specifically in approaches to gravity involving the presence of geometry–matter coupling [144]. Examples of such theories are the $f(R, L_m)$ [145] and the $f(R, T)$ [146] theories.

The non-conservation of the matter energy–momentum tensor, as shown, for example, for the Barthel–Randers case by Equation (68), can thus be interpreted as showing that due to the existence of the Finslerian geometric effects, during cosmological evolution, matter creation processes may take place. This indicates the possibility of creating matter from geometry. Quantum field theories in curved spacetime also predict the same particle creation effect, as initially proposed and investigated in [147–152]. In quantum field theory, particle creation is due to the time variation of the gravitational field. In an anisotropic Bianchi Type I metric, quantum particle creation was considered in [149], and for a quantum scalar field with a non-zero mass, the renormalized expression of the energy–momentum tensor was determined. Hence, the osculating Finsler–Barthel-type gravity theories, in which the creation of matter is also allowed by the general formalism, could also be interpreted as providing an effective, semiclassical description of the quantum effects in the gravitational field. It is important to note, however, that the nature of the particles is not necessarily known, unless quantum theoretical effects are taken into account.

3.6.1. Irreversible Thermodynamics and Matter Creation

Equation (68), obtained within the framework of the Barthel–Randers cosmology, shows that the covariant divergence of the energy–momentum tensor, which is a function of the equilibrium quantities of the thermodynamic system represented by the baryonic matter, is different from zero. Similar effects appear for the case of other thermodynamical quantities, like, for example, the particle and entropy fluxes. Hence, in the presence of matter creation, all the balance equilibrium equations must be modified to account for this effect [153–155]. We will present first the general formalism of irreversible thermodynamics in the presence of matter creation, by adopting a cosmological perspective. We will consider all the results in the Riemann space, with metric $a_{AB}(x)$. Moreover, we interpret the Finslerian effects as generating a set of specific physical events in the background Riemann geometry. Hence, in the following, all the physical and geometrical quantities will be expressed with the help of the FLRW metric (56). Consequently, all considered physical and geometrical quantities are functions of the cosmological time t only.

Particle balance equations.

To describe particle dynamics, we introduce the particle number density n, and the four-velocity u^I of matter. From these quantities, we construct the particle flux $N^I \equiv nu^I$. All these physical parameters are defined in Riemannian geometry. The particle balance equation in the presence of matter creation is given by

$$\nabla_I N^I = \dot{n} + 3Hn = n\Gamma, \tag{88}$$

where ∇_I is the covariant derivative defined in the Riemann space with the help of the Levi–Civita connection associated with the FLRW metric (56), while Γ denotes the matter creation rate. For $\Gamma \ll 3H$, the source term in the particle balance equation is negligible, and we reobtain the standard particle conservation law of general relativity.

The entropy flux.

We now introduce the entropy density $\tilde{s}$, and the entropy per particle $\sigma = \tilde{s}/n$. From these quantities we construct the entropy flux vector defined as $S^I \equiv \tilde{s}u^I = n\sigma u^I$. The divergence of the entropy flux gives the relation

$$\nabla_I S^I = n\dot{\sigma} + n\sigma\Gamma \geq 0, \tag{89}$$

where the positivity condition is a direct consequence of the second law of thermodynamics. The case $\sigma =$ constant gives the relation

$$\nabla_I S^I = n\sigma\Gamma = \tilde{s}\Gamma \geq 0. \tag{90}$$

Equation (90) shows that if the entropy per particle can be taken as a constant, then the variation of the entropy is only due to the matter generated via the transfer of the energy of the gravitational field to matter. Since $\tilde{s} > 0$, the particle production rate Γ must satisfy the basic thermodynamic condition $\Gamma \geq 0$. From a physical point of view, this condition can be interpreted as permitting the creation of matter from the gravitational field, but suppressing the opposite process.

The creation pressure.

If particle creation takes place, the matter energy–momentum tensor must also be modified to take into account the presence of the irreversible processes and the second law of thermodynamics. Generally, in the thermodynamical description of open systems, the energy–momentum tensor can be represented as [156]

$$T^{IJ} = T^{IJ}_{\rm eq} + \Delta T^{IJ}, \tag{91}$$

where $T^{IJ}_{\rm eq}$ is the equilibrium thermodynamic component [156], and ΔT^{IJ} describes the supplementary terms induced by particle creation. For a homogeneous and isotropic spacetime geometry, ΔT^{IJ}, giving the particle creation contribution to T^{IJ}, can be generally represented in the form

$$\Delta T^0_0 = 0, \quad \Delta T^J_I = -P_c\delta^J_I, \tag{92}$$

where P_c denotes the creation pressure, an effective thermodynamic quantity, which in a macroscopic physical system describes phenomenologically particle creation. Moreover, in a fully covariant representation, the tensor ΔT^{IJ} is given by [156]

$$\Delta T^{IJ} = -P_c h^{IJ} = -P_c\left(a^{IJ} - u^I u^J\right), \tag{93}$$

where $h^{IJ} = a^{IJ} - u^I u^J$ is the projection operator defined in the FLRW geometry. Thus, we straightforwardly obtain the relation $u_I\nabla_J\Delta T^{IJ} = 3HP_c$.

In the presence of particle production by the gravitational field, from the scalar component of the energy balance equation $u_I\nabla_J T^{IJ} = 0$, obtained from Equation (91), we obtain the time variation of the energy density ρ of the cosmological fluid as

$$\dot{\rho} + 3H\left[\rho + \frac{1}{c^2}(p + P_c)\right] = 0. \tag{94}$$

The thermodynamic quantities describing baryonic matter must also satisfy the Gibbs law [154]

$$nTd\left(\frac{\tilde{s}}{n}\right) = nTd\sigma = d\rho - \frac{\rho + p/c^2}{n}dn, \tag{95}$$

where T is the temperature of the cosmological matter.

3.6.2. Application: Particle Creation in Barthel–Randers Cosmology

As an example of the application of the irreversible thermodynamic of open systems, we consider now the interpretation of the Barthel–Randers cosmology as a cosmological theory also describing particle creation during the evolution of the Universe.

Creation pressure in Barthel–Randers cosmology.

After some simple algebraic transformations, the particle energy balance Equation (68) of the Barthel–Randers cosmology can be rewritten as

$$\dot{\rho} + 3H\left[\left(\rho + \frac{p}{c^2}\right)\left(1 + \frac{\dot{\phi}}{2H\phi}\right)\right] = 0. \tag{96}$$

By comparing Equations (94) and (96), we find the expression of the Barthel–Randers creation pressure as

$$P_c = \frac{\dot{\phi}}{2H\phi}\left(\rho c^2 + p\right) = \frac{c^2\rho\dot{\phi}}{2H\phi}(1+\omega), \tag{97}$$

where $\omega = p/\rho c^2$. The energy density balance Equation (68) can now be derived equivalently from the divergence of the total energy momentum tensor T^{IJ}, given by

$$T^{IJ} = \left(\rho c^2 + p + P_c\right)u^I u^J - (p + P_c)a^{IJ}, \tag{98}$$

where all the mathematical operations must be performed in the Riemann space with the FLRW metric (56).

The particle creation rate.

By assuming adiabatic particle production, which requires that $\dot{\sigma} = 0$, the Gibbs relation (95) gives

$$\dot{\rho} = \left(\rho + \frac{p}{c^2}\right)\frac{\dot{n}}{n} = \left(\rho + \frac{p}{c^2}\right)(\Gamma - 3H). \tag{99}$$

By combining this relation with the energy balance Equation (96), we obtain the particle creation rate as a function of the creation pressure, the Hubble function and the equilibrium thermodynamic quantities as

$$\Gamma = \frac{-3HP_c}{\rho c^2 + p}. \tag{100}$$

By using Equation (97), we find for the Barthel–Randers cosmological particle creation rate the expression

$$\Gamma = -\frac{3}{2}\frac{\dot{\phi}}{\phi} = -\frac{3}{2}\frac{d}{dt}\ln\phi = -\frac{3}{2}\frac{\dot{a}\eta + a\dot{\eta}}{1 + a\eta}. \tag{101}$$

If $1 + a\eta > 0$, the condition $\Gamma \geq 0$, which is equivalent with the existence of particle creation, leads to the constraint

$$\dot{\phi} = \dot{a}\eta + a\dot{\eta} = a(\dot{\eta} + H\eta) \leq 0, \tag{102}$$

on the scale factor a, and the temporal component of the one-form η. The condition does not depend explicitly on the equation of state of the baryonic matter, but an indirect dependence via the Hubble function does exist. The condition $\dot{\phi} < 0$ implies the existence of a negative creation pressure, as it follows from Equation (97). Therefore particle production is thermodynamically allowed only if the creation pressure is negative, $P_c < 0$.

The Barthel–Randers particle balance equation can thus be reformulated to take the form

$$\dot{n} + 3Hn = -\frac{3}{2} n \frac{\dot{\phi}}{\phi} = \Gamma n, \tag{103}$$

and it can be integrated to give the expression for the particle number density

$$n = \frac{n_0}{\phi^{3/2} a^3}, \tag{104}$$

where n_0 is a constant of integration.

For a Universe consisting of pressureless dust with $p = 0$, the creation pressure is given by

$$P_c = \frac{\dot{\phi}}{2H\phi} \rho c^2 = \frac{\rho c^2}{2H} \frac{d}{dt} \ln \phi, \tag{105}$$

and it depends linearly on the baryonic matter density.

The divergence of the entropy flux vector S^I takes the form

$$\nabla_I S^I = \frac{-3n\sigma H P_c}{\rho c^2 + p} = -\frac{3}{2} n\sigma \frac{\dot{\phi}}{\phi} = n\sigma\Gamma. \tag{106}$$

The matter temperature.

The temperature T of the baryonic matter represents an important characteristic of physical systems. To obtain the temperature evolution in the presence of particle creation, we consider the general thermodynamic case in which the density and the pressure are functions of the particle number density, and of the temperature. Hence ρ and p can be generally represented in parametric form $\rho = \rho(n, T)$ and $p = p(n, T)$, respectively. Then, we obtain

$$\dot{\rho} = \left(\frac{\partial \rho}{\partial n}\right)_T \dot{n} + \left(\frac{\partial \rho}{\partial T}\right)_n \dot{T}. \tag{107}$$

By using the energy and particle balance equations, we find first the relation

$$-3H\left(\rho c^2 + p + P_c\right) = \left(\frac{\partial \rho}{\partial n}\right)_T n(\Gamma - 3H) + \left(\frac{\partial \rho}{\partial T}\right)_n \dot{T}. \tag{108}$$

As a second step we use the thermodynamic relation [156]

$$T\left(\frac{\partial p}{\partial T}\right)_n = \rho c^2 + p - n\left(\frac{\partial \rho}{\partial n}\right)_T, \tag{109}$$

which together with Equation (108) gives the temperature evolution of the matter in the Barthel–Randers cosmology in the presence of particle production as

$$\frac{\dot{T}}{T} = \frac{1}{c^2}\left(\frac{\partial p}{\partial \rho}\right)_n \frac{\dot{n}}{n} = \omega \frac{\dot{n}}{n}. \tag{110}$$

From the particle balance equation, we obtain the ratio $\dot{n}/n$ as

$$\frac{\dot{n}}{n} = -3\left(\frac{\dot{\phi}}{\phi} + \frac{\dot{a}}{a}\right). \tag{111}$$

By assuming that $\dot{\phi} < 0$, we obtain for the temperature evolution of the particles in the Barthel–Randers Universe the relation

$$T = T_0 \frac{\phi^{3\omega/2}}{a^3}. \tag{112}$$

Generally, ω is an arbitrary scale factor-dependent parameter $\omega = \omega(a)$ [157]. In a thermodynamically consistent cosmological model, all geometrical and physical quantities must be well-defined and regular for all $\omega(a)$.

3.6.3. Creation of Exotic Matter

In our discussion of the thermodynamics of open systems, as presented in the previous section, we have assumed that matter is created in the form of baryonic matter, satisfying the energy condition $\rho c^2 + p \geq 0$, and the restriction on the parameter of the matter equation of state $\omega \geq 0$. But we cannot a priori exclude the possibility case in which an exotic fluid with $\omega < 0$ is created during the cosmological evolution of the Barthel–Randers Universe. The open system thermodynamic approach to particle creation considered previously is also applicable if $\omega < 0$. For this case the creation pressure becomes negative for $\dot{\phi} > 0$, with the particle creation rate Γ becoming positive. Therefore, matter creation processes generating exotic particles can also be included in the Barthel–Randers cosmological model.

A particular and important case is represented by an exotic fluid satisfying the equation of state $\rho_{(ex)}c^2 + p_{(ex)} = 0$, with $\omega = -1$, which is equivalent to the presence of a cosmological constant. Then from Equation (94), we obtain

$$\dot{\rho}_{(ex)} = -3HP_c. \tag{113}$$

If the exotic particle creation process is adiabatic, with $\dot{\sigma} = 0$, from the Gibbs relation, we find

$$\dot{\rho}_{(ex)} = \left(\rho_{(ex)}c^2 + p_{(ex)}\right)\frac{\dot{n}_{(ex)}}{n_{(ex)}} = 0. \tag{114}$$

The above two equations independently give

$$\dot{\rho}_{(ex)} = P_c = 0, \tag{115}$$

which describe a Universe with constant exotic matter density and vanishing creation pressure. On the other hand, if $\omega = -2$, and $\rho_{(ex)} > 0$, then $P_c = -\left(c^2\dot{\phi}/2H\phi\right)\rho_{(ex)}$, $\Gamma = (3/2)\dot{\phi}/\phi$, and matter production can take place if the conditions $\dot{\phi} > 0$ and $\phi > 0$ are satisfied.

Thus, in a Barthel–Randers Universe, the creation of exotic matter or possibly of scalar fields is allowed in a way consistent with the laws of thermodynamics. The creation processes take place in the Riemannian geometry characterized by the FLRW metric.

4. Cosmological Implications of Barthel–Randers and Barthel–Kropina Models

In this section, we investigate the cosmological implications of the Barthel–Randers and Barthel–Kropina models by exploring three distinct variants of the Barthel–Randers framework alongside the Barthel–Kropina cosmological model. To constrain the free parameters of these models, we employ a combination of observational datasets, including Type Ia Supernovae, Baryon Acoustic Oscillations, and Hubble parameter measurements. By extracting the posterior distributions of the model parameters through Bayesian inference, we are able to assess the observational viability of the Barthel–Randers and Barthel–Kropina models. This comparison with the standard ΛCDM cosmology enables us to explore possible deviations from the conventional expansion history and to evaluate whether these geometrically extended models offer a competitive or improved description of the Universe's evolution.

4.1. Specific Cosmological Models

In this subsection, we present the normalized Hubble functions associated with both the Barthel–Randers [120] and Barthel–Kropina [121] cosmological models. Our starting point is the family of cosmological scenarios proposed in [120], where three distinct variants of the Barthel–Randers model were introduced. Each of these variants is characterized by a specific choice of the function $\varphi(z)$. The normalized Hubble function for all three models can be expressed in a unified form as

$$h(z) = \frac{2\varphi(z)\sqrt{(1+z)^3\sqrt{\varphi(z)}\,\Omega_{m0} + \varphi(z)^2\Omega_{\Lambda 0} + (1+z)^4\Omega_{r0}}}{(1+z)\frac{d\varphi(z)}{dz} - 2\varphi(z)}, \tag{116}$$

where z is the redshift, and Ω_{m0}, $\Omega_{\Lambda 0}$, and Ω_{r0} are the present-day matter, dark energy, and radiation density parameters, respectively. The dark energy density parameter $\Omega_{\Lambda 0}$ is obtained through the constraint

$$\Omega_{\Lambda 0} = \left(1 - \frac{1}{2}\varphi'(0)\right)^2 - \Omega_{m0} - \Omega_{r0}, \tag{117}$$

where $\varphi'(0)$ is the derivative of the function $\varphi(z)$ evaluated at $z = 0$. The form of $\varphi(z)$ determines the behavior of each specific model and encodes the influence of the underlying Finslerian geometry. In the following, we present the explicit forms of $\varphi(z)$ corresponding to each of the three models proposed in [120]:

1. **Linear model:** $\varphi(z) = 1 + \beta z$.
2. **Logarithmic model:** $\varphi(z) = 1 + \ln(1 + \beta z)$.
3. **Exponential model:** $\varphi(z) = e^{2\beta z}$.

We can obtain the corresponding normalized Hubble function by plugging the corresponding form of $\varphi(z)$ into Equation (116).

In the case of the Barthel–Kropina geometry, we adopt the model proposed by [121]. The corresponding normalized Hubble function is expressed as a system of differential equations in the redshift representation as follows:

$$\frac{df(z)}{dz} = -\frac{u(z)}{(1+z)h(z)}, \tag{118}$$

$$\begin{aligned}\frac{du(z)}{dz} = \frac{1+f(z)}{2(1+z)h(z)}\Bigg[&2h(z)\left(\frac{2}{1+f(z)} - 3\omega(1+f(z))\right)u(z) \\ &+ 3\left(\omega - \frac{1}{(1+f(z))^2}\right)u(z)^2 + 3\omega f(z)(2+f(z))h(z)^2\Bigg],\end{aligned} \tag{119}$$

$$\frac{dh(z)}{dz} = \frac{1}{2(1+z)h(z)}\left[3h(z)^2 - \frac{4h(z)u(z)}{1+f(z)} + \frac{3u(z)^2}{(1+f(z))^2} + \frac{2(1+z)h(z)}{1+f(z)}\frac{du(z)}{dz}\right]. \tag{120}$$

The system of equations above has to be solved with initial conditions $f(0) = f_0$, $u(0) = u_0$, and $h(0) = 1$.

4.2. Methodology and Datasets

In this subsection, we provide a detailed explanation of the methodology used to estimate the posterior distributions of the model parameters, employing the Markov Chain Monte Carlo (MCMC) approach. This approach allows us to constrain model parameters by analyzing various observational datasets. The MCMC method explores the parameter space of theoretical models by sampling from the likelihood function and incorporating prior information, leading to a robust estimation of the posterior probability distribution [158].

Through this method, the model's parameter space is thoroughly explored. The MCMC algorithm relies on Bayes' theorem, which is given by

$$P(\theta|D) = \frac{L(D|\theta)P(\theta)}{P(D)}, \tag{121}$$

where $P(\theta|D)$ represents the probability of the parameters θ given the observational data D. The term $L(D|\theta)$ is the likelihood function, which measures how well the model fits the data. $P(\theta)$ is the prior distribution, incorporating any previous knowledge about the parameters, while $P(D)$ is the evidence, acting as a normalization factor [159].

One of the key advantages of the MCMC method is that it not only finds the most likely values for the parameters but also accounts for uncertainties in both the models. We define the likelihood function in such a way that it compares the theoretical predictions of the Hubble parameter ($H(z)$), luminosity distance ($\mu(z)$), transverse distance ($D_H(z)$), comoving angular diameter distance ($D_M(z)$), and comoving volume distance ($D_V(z)$) with observational data, taking into account uncertainties through covariance matrices.

The MCMC sampling is carried out using the `emcee` library[1] [160,161], which includes an affine-invariant ensemble sampler. This sampler is used to efficiently explore the parameter space. Specifically, we use 30 walkers, with a total of 100,000 steps for the chain. To ensure the removal of biases, the first 10,000 steps are discarded as burn-in, and the remaining steps are thinned by a factor of 30 to reduce autocorrelation between samples.

After running the MCMC chains, the posterior distributions of the parameters are analyzed, and the best-fit values are identified. To visualize and analyze the posterior distributions, we utilize the `GetDist` package[2] [162], which provides an extensive set of tools for generating 1D and 2D posterior distributions. In this work, we use three different observational datasets: Cosmic Chronometers, Type Ia Supernovae, and Baryon Acoustic Oscillations.

Below, we provide a detailed description of each dataset and how the likelihood has been formed based on them.

- **Cosmic Chronometers:** In this study, we use the Hubble measurements extracted based on the differential age approach. This technique leverages passively evolving massive galaxies, which formed at redshifts around $z \sim 2-3$, enabling a direct and model-independent determination of the Hubble parameter using the relationship $\Delta z/\Delta t$. This method significantly reduces the reliance on astrophysical assumptions [163]. For our analysis, we use 15 Hubble measurements selected from the 31 Hubble measurements, which cover a redshift range from $0.179 \leq z \leq 1.965$ [164–166]. We use the likelihood function provided by Moresco in his GitLab repository[3] which uses the full covariance matrix, accounting for both statistical and systematic uncertainties [167,168] .
- **Type Ia Supernova:** We also use the Pantheon$^+$ dataset without the SHOES calibration, which consists of 1701 light curves from 1550 Type Ia Supernovae (SNe Ia) covering a redshift range of $0 \leq z \leq 2.3$ [169]. To analyze this data, we adopt the likelihood function described in [170], which incorporates the total covariance matrix, $\mathbf{C}_{\text{total}}$, which includes both statistical ($\mathbf{C}_{\text{stat}}$) and systematic ($\mathbf{C}_{\text{sys}}$) uncertainties [171]. The likelihood function is given by $\mathcal{L}_{\text{SNe Ia}} = e^{\left(-\frac{1}{2}\mathbf{r}^T\mathbf{C}_{\text{total}}^{-1}\mathbf{r}\right)}$, where $\mathbf{r}$ represents the residual vector, defined as the difference between the observed and theoretical distance moduli: $r_i = \mu_{\text{obs}}(z_i) - \mu_{\text{th}}(z_i, \theta)$, where θ. Here, $\mathbf{C}_{\text{total}}^{-1}$ is the inverse of the total covariance matrix. The model-predicted distance modulus is calculated as $\mu_{\text{model}}(z_i) = 5\log_{10}\left(\frac{d_L(z)}{\text{Mpc}}\right) + \mathcal{M} + 25$, where the luminosity distance $d_L(z)$ in a flat FLRW Universe is given by $d_L(z) = c(1+z)\int_0^z \frac{dz'}{H(z')}$. Here, c is the speed of light,

and $H(z)$ is the Hubble parameter. This formulation highlights the degeneracy between the nuisance parameter $\mathcal{M}$ and the Hubble constant H_0.

- **Baryon Acoustic Oscillation:** In our analysis, we also include the 13 recent Baryon Acoustic Oscillation (BAO) measurements from the Dark Energy Spectroscopic Instrument (DESI) Data Release 2 (DR2) [172]. These measurements cover a redshift range of $0.295 \leq z \leq 2.330$. They were obtained from observations of the Bright Galaxy Sample (BGS), Luminous Red Galaxies (LRG1, LRG2, LRG3), Emission Line Galaxies (ELG1 and ELG2), Quasars (QSO), and Lyman-α tracers[4]. The measurements are reported using three distance indicators: the Hubble distance $D_H(z)$, the comoving angular diameter distance $D_M(z)$, and the volume-averaged distance $D_V(z)$. To compare these with cosmological models, we compute the ratios $D_H(z)/r_d$, $D_M(z)/r_d$, and $D_V(z)/r_d$, where r_d represents the sound horizon at the drag epoch, occurring around redshift $z \sim 1060$. In a flat ΛCDM model, $r_d = 147.09 \pm 0.26$ Mpc [72]. However, in this study, we treat r_d as a free parameter, allowing late-time observations to constrain the corresponding model parameters [173–177]. The chi-squared statistic for the BAO measurements is given by $\chi^2_i = (\vec{O}_i^{\,\text{th}} - \vec{O}_i^{\,\text{obs}})^T \, \mathbf{C}_i^{-1} \, (\vec{O}_i^{\,\text{th}} - \vec{O}_i^{\,\text{obs}})$, where $\vec{O}_i^{\,\text{th}}$ and $\vec{O}_i^{\,\text{obs}}$ denote the vectors of theoretical predictions and observed measurements, respectively, and $\mathbf{C}_i$ is the associated covariance matrix[5].

The posterior distribution of model parameters is obtained by maximizing the likelihood function. The total likelihood function is given by

$$\mathcal{L}_{\text{tot}} = \mathcal{L}_{\text{CC}} \times \mathcal{L}_{\text{SNe Ia}} \times \mathcal{L}_{\text{BAO}}. \tag{122}$$

First, we discuss how to extract the posterior distribution of the model parameters in the Barthel–Randers framework. To achieve these, we apply the standard approach outlined above. In these models, we treat the parameters H_0, Ω_{m0}, β, $\mathcal{M}$, and r_d as free parameters with the following priors: H_0 $(\text{km}\,\text{s}^{-1}\,\text{Mpc}^{-1}) \in [50, 100]$, $\Omega_{mo} \in [0, 1]$, $\mathcal{M} \in [-20, -18]$, r_d $(\text{Mpc}) \in [100, 200]$, and $\beta \in [0, 0.1]$, as the model is sensitive to this parameter. The Ω_{r0} is extracted using the following relation: $\Omega_{r0} = \left(4.183699 \times 10^{-5}\right) h^{-2}$, where $h = \frac{H_0}{100}$. In the case of the linear and logarithmic models, $\Omega_{\Lambda 0}$ is extracted using the relation $\Omega_{\Lambda 0} = 1 - \beta + \frac{\beta^2}{4} - \Omega_{m0} - \Omega_{r0}$, while in the case of the exponential model, $\Omega_{\Lambda 0}$ is extracted using the relation $\Omega_{\Lambda 0} = 1 - 2\beta + \beta^2 - \Omega_{m0} - \Omega_{r0}$. This makes the explicit variation of Ω_{r0} and $\Omega_{\Lambda 0}$ redundant, as both are fully determined by the other parameters.

To constrain the Barthel–Kropina model, we begin by numerically solving the system of differential equations given in Equations (118)–(120). These equations are integrated using the *solve_ivp* function from *SciPy*, employing the Radau method with a fifth-order implicit Runge–Kutta scheme particularly effective for handling the stiff differential equations. For numerical stability and accuracy over the redshift range $z \in [0, 3]$, we set the relative and absolute tolerances to 10^{-3} and 10^{-6}, respectively. After obtaining the numerical solutions, we use an MCMC approach to constrain the model parameters. For more information on how to handle these kinds of Hubble-like functions that appear within differential equations, please consult [178]. In the case of the Barthel–Kropina model, we take the H_0 $(\text{km}\,\text{s}^{-1}\,\text{Mpc}^{-1}) \in [50, 100]$, $u_o \in [0.0, 3.0]$, $\mathcal{M} \in [-20, -18]$, r_d $(\text{Mpc}) \in [100, 200]$, and $f_0 \in [0, 0.1]$. It is important to note that in both cases, we work with the normalized Hubble function. The final Hubble parameter $H(z)$ can be obtained by multiplying the normalized function $h(z)$ by the Hubble constant H_0, i.e., $H(z) = H_0 \cdot h(z)$.

Convergence Test

Gelman–Rubin Statistic $\left(\widehat{R}\right)$

To assess the convergence of multiple MCMC chains, we use the Gelman–Rubin criterion $\left(\widehat{R}\right)$, which compares the within-chain variance $\left(\widehat{W}\right)$ and the between-chain variance (B) to estimate the total variance $\left(\widehat{V}\right)$. These quantities are related by

$$\widehat{R} = \sqrt{\frac{\widehat{V}}{\widehat{W}}}. \tag{123}$$

If $\widehat{R} \approx 1$, it indicates convergence, suggesting that the chains are sampling from the same distribution. On the other hand, if $\widehat{R} > 1$, it suggests non-convergence, and values significantly above 1 (e.g., $\widehat{R} > 1.1$) indicate that more iterations are needed to ensure proper convergence.

Convergence of Chains and Trace Plots

In addition to the Gelman–Rubin statistic, trace plots are used to visualize whether the chains have converged. These plots show the evolution of each parameter over time, helping to verify if the chains are evolving in the convergence region or still exploring different regions of the parameter space.

5. Comparing Barthel–Randers, Barthel–Kropina and ΛCDM Models

After obtaining the mean parameter values from the MCMC simulations, we proceed to compare the predictions of the Barthel–Randers and Barthel–Kropina cosmological models with those of the standard ΛCDM model. This comparison is essential to assess how well the Barthel–Randers and Barthel–Kropina frameworks are consistent with the observed cosmic expansion history.

5.1. Evolution of the Hubble Parameter, Hubble Residual, and BAO Distance Scales

In this subsection, we compare the Hubble parameter $H(z)$ predicted by three Barthel–Randers models and the Barthel–Kropina model with those of the standard ΛCDM model. The ΛCDM model is given by the equation

$$H_{\Lambda\mathrm{CDM}}(z) = H_0\sqrt{\Omega_{m0}(1+z)^3 + \Omega_{\Lambda 0}},$$

where $H_0 = 67.8\,\mathrm{km\,s^{-1}\,Mpc^{-1}}$, $\Omega_{m0} = 0.3092$, and $\Omega_{\Lambda 0} = 0.608$. To quantify the deviation between the Barthel–Randers models and ΛCDM, we define the Hubble residual as

$$\Delta H(z) = H_{\text{Barthel-Randers Models}}(z) - H_{\Lambda\mathrm{CDM}}(z),$$

where $H_{\text{Barthel-Randers Models}}(z)$ denotes the Hubble parameter predicted by the respective Barthel–Randers model. Similarly, for the Barthel–Kropina model, we define

$$\Delta H(z) = H_{\text{Barthel-Kropina Model}}(z) - H_{\Lambda\mathrm{CDM}}(z),$$

where $H_{\text{Barthel-Kropina Model}}(z)$ denotes the Hubble parameter predicted by the respective Barthel–Kropina model. We plot both $H(z)$ and $\Delta H(z)$ for the Barthel–Randers models and Barthel–Kropina model. A small or nearly constant residual indicates close agreement with the ΛCDM model, while significant deviations suggest potential extensions to the standard cosmological model. In addition to analyzing the Hubble parameter, we also consider the BAO distance scales, specifically the ratio between the angle-averaged distance

$D_V(z) = (zD_M^2 D_H)^{1/3}$ and the ratio of transverse to line-of-sight comoving distances, $FAP(z) = D_M/D_H$, which are scaled by $z^{-2/3}$ and z^{-1}, respectively. By comparing these BAO distance ratios with the predictions of the best-fit flat ΛCDM model, we gain further insight into the behavior of the Barthel–Randers and Barthel–Kropina models in relation to the standard cosmological framework. The results of these comparisons are visualized by plotting $H(z)$, $\Delta H(z)$, and the BAO distance scales, providing a comprehensive view of how each model behaves relative to ΛCDM. We consider the CC data [164–166] in our analysis, and the BAO measurements are taken from [172].

5.2. Cosmographic Analysis of Barthel–Randers and Barthel–Kropina Models

Cosmography provides a model-independent framework to describe the kinematic behavior of the Universe by expanding cosmological quantities in terms of redshift [179–182]. In this work, we apply this approach to analyze the deceleration and jerk parameters within the Barthel–Randers and Barthel–Kropina cosmological models, which modify standard cosmic dynamics through different geometrical correction terms.

Deceleration Parameter $q(z)$ and Jerk Parameter $j(z)$

The deceleration parameter $q(z)$ describes the acceleration or deceleration of the cosmic expansion and is defined as

$$q(z) = -\frac{1}{H^2(z)}\frac{dH(z)}{dz} - 1.$$

A negative value of $q(z)$ indicates that the Universe is undergoing accelerated expansion. Two important phases derived from $q(z)$ are the present-day deceleration parameter, $q_0 = q(z = 0)$, which describes the current rate of acceleration, and the transition redshift, $z_{\rm tr}$, defined by the condition $q(z_{\rm tr}) = 0$, marking the point at which the Universe transitioned from decelerated to accelerated expansion. The jerk parameter $j(z)$ is a third-order cosmographic quantity defined as [183]

$$j(z) = \frac{1}{H^3(z)}\frac{d^2H(z)}{dz^2},$$

which characterizes the rate of change of the acceleration. Importantly, in the standard ΛCDM model, the jerk parameter remains constant at $j(z) = 1$. Any deviation from this value can signal dynamics beyond the standard cosmological model. For the three Barthel–Randers models and the Barthel–Kropina model, we evaluate both the deceleration parameter $q(z)$ and the jerk parameter $j(z)$ numerically and assess their behavior across the redshift range.

5.3. Statistical Assessment of Barthel–Randers and Barthel–Kropina Models

In this subsection, we apply a set of model selection criteria to evaluate the goodness of fit and model complexity of three variants of the Barthel–Randers cosmological models (linear, logarithmic and exponential) and Barthel–Kropina model. It is crucial to assess how well each model aligns with the data when compared to the ΛCDM model.

5.4. Goodness of Fit

The primary measure of model fit is the chi-squared statistic, χ^2, which quantifies the discrepancy between theoretical predictions and observational data. For a suitable comparison, as models generally have different numbers of parameters, we compute the reduced chi-square

$$\chi^2_{\rm red} = \frac{\chi^2_{\rm tot}}{\rm DOF}, \tag{124}$$

where χ^2_{tot} is the total chi-squared value and DOF denotes the degrees of freedom, calculated as the number of data points minus the number of fitted parameters. A value of $\chi^2_{\text{red}} \approx 1$ indicates a good statistical fit [184]. Lower values can suggest overfitting, while significantly higher values may reflect poor model performance.

5.4.1. Model Comparison Using AIC and BIC

In addition to chi-squared statistics, we apply information criteria that account for both fit quality and model complexity. These include the Akaike information criterion (AIC) and the Bayesian information criterion (BIC), defined respectively as [185–189]

$$\text{AIC} = -2\log\mathcal{L}_{tot,max} + 2\mathcal{P}, \tag{125}$$

$$\text{BIC} = -2\log\mathcal{L}_{tot,max} + \mathcal{P}\ln(\mathcal{N}), \tag{126}$$

where $\mathcal{P}$ is the number of free parameters, $\mathcal{N}$ is the total number of data points used in the analysis and $\mathcal{L}_{tot,max}$ is the total maximum likelihood. In our analysis, the total number of data points used is the sum of three different observational datasets: $\mathcal{N} = 1729$. For the model comparison, we note that the ΛCDM model has four free parameters, whereas the Barthel–Randers cosmological model has five free parameters, and the Barthel–Kropina model has six free parameters. These criteria penalize overly complex models to prevent overfitting. BIC generally applies a stricter penalty than AIC, especially in large datasets.

5.4.2. Relative Comparison: ΔAIC and ΔBIC

To directly compare the Barthel–Randers models with the ΛCDM model, we compute

$$\Delta\text{AIC} = \text{AIC}_{\text{Barthel-Randers Models}} - \text{AIC}_{\Lambda\text{CDM Model}}, \tag{127}$$

$$\Delta\text{BIC} = \text{BIC}_{\text{Barthel-Randers Models}} - \text{BIC}_{\Lambda\text{CDM Model}}. \tag{128}$$

Similarly, for the comparison between the Barthel–Kropina model and the ΛCDM model, we compute

$$\Delta\text{AIC} = \text{AIC}_{\text{Barthel-Kropina Model}} - \text{AIC}_{\Lambda\text{CDM Model}}, \tag{129}$$

$$\Delta\text{BIC} = \text{BIC}_{\text{Barthel-Kropina Model}} - \text{BIC}_{\Lambda\text{CDM Model}}. \tag{130}$$

According to the calibrated Jeffreys' scales [190], these differences offer insight into model preference:

- $|\Delta\text{AIC}| \leq 2$: Comparable support.
- $4 \leq |\Delta\text{AIC}| < 10$: Considerably less support.
- $|\Delta\text{AIC}| \geq 10$: Strongly disfavored.
- $|\Delta\text{BIC}| \leq 2$: Weak evidence against the model.
- $2 < |\Delta\text{BIC}| \leq 6$: Moderate evidence against the model.
- $|\Delta\text{BIC}| > 6$: Strong evidence against the model.

A negative value of ΔAIC or ΔBIC indicates that the Barthel–Randers and Barthel–Kropina models are preferred over ΛCDM, whereas positive values indicate that these models are less favored

5.4.3. *p*-Value Statistics

In our analysis, we also computed the *p*-value to assess the statistical significance of the fit for the studied cosmological models, calculated as follows:

$$p = 1 - \mathcal{F}_{\chi^2_{\text{min}}}(\chi \mid \nu),$$

where $\mathcal{F}_{\chi^2_{\min}}(\chi \mid \nu)$ is the cumulative distribution function (CDF) of the chi-squared distribution with ν degrees of freedom, and ν represents the number of data points minus the number of free parameters [191].

The p-value quantifies the likelihood of observing results as extreme as those seen in the data, assuming the null hypothesis holds true. A p-value smaller than 0.05 ($p < 0.05$) indicates statistical significance, providing strong evidence against the null hypothesis and suggesting that the model is a good fit for the data. These corresponding statistical metrics ($\chi^2_{\min}$, χ^2_{red}, AIC, BIC, ΔAIC, ΔBIC, and p-value) are computed and compared with those of the ΛCDM model. These statistical metrics ensure that both the goodness of fit and the complexity of each model are thoroughly evaluated, enabling a comprehensive statistical assessment of the Barthel–Randers and Barthel–Kropina models in the context of cosmology.

6. Summary and Discussion of the Results

In the present section, we discuss the main results obtained by confronting the proposed cosmological models with observations, and by comparing their predictions and statistical significance with those of the ΛCDM model

6.1. MCMC and Convergence Results

Figure 2 shows the corner plot of the parameters of the Barthel–Randers and Barthel–Kropina models. The diagonal panels illustrate the one-dimensional marginalized posterior distributions for each parameter, highlighting their most probable values. The off-diagonal panels depict the two-dimensional marginalized contour plots, showing the 68% and 95% confidence intervals. These contour plots also reveal correlations or degeneracies between each model parameter. Figure 3 shows the corresponding trace plots, which depict the convergence behavior of the Markov chains for each parameter. As a convergence diagnostic, the Gelman–Rubin statistic was used for each model parameter. The results obtained are given by

$$\mathrm{BR}^{\text{Gelman-Rubin statistics}}_{\text{Linear Case}}\{H_0, \Omega_{mo}, b_1, \mathcal{M}, r_d\} = \{1.006, 1.001, 1.001, 1.006, 1.006\},$$

$$\mathrm{BR}^{\text{Gelman-Rubin statistics}}_{\text{Logarithmic Case}}\{H_0, \Omega_{mo}, b_1, \mathcal{M}, r_d\} = \{1.005, 1.002, 1.001, 1.005, 1.005\},$$

$$\mathrm{BR}^{\text{Gelman-Rubin statistics}}_{\text{Exponential Case}}\{H_0, \Omega_{mo}, b_1, \mathcal{M}, r_d\} = \{1.004, 1.002, 1.001, 1.004, 1.004\},$$

$$\mathrm{BK}^{\text{Gelman-Rubin statistics}}\{H_0, f_0, u_0, \omega, \mathcal{M}, r_d\} = \{1.007, 1.001, 1.002, 1.002, 1.0071.007\}.$$

In our case, the $\widehat{R}$ values for the Barthel–Randers (linear, logarithmic, and exponential) and Barthel–Kropina models are all very close to 1, indicating excellent convergence of the MCMC chains. However, it is important to note that in the BR models, $\Omega_{\Lambda 0}$ and Ω_{r0} are not independent parameters. Instead, they are determined algebraically once the other parameters constrained through the MCMC analysis are known. For this reason, we do not list $\Omega_{\Lambda 0}$ and Ω_{r0} among the constrained parameters, as they are derived quantities rather than directly fitted ones.

One can observe that the predicted values of H_0 from the ΛCDM and Barthel–Randers models (linear, logarithmic, and exponential cases), as well as from the osculating Barthel–Kropina dark energy model, are in close agreement with those obtained from Moresco's results. Specifically, Moresco's measurements, considering both the full covariance matrix and without systematics, are as follows: Without systematics: $H_0 = 66.2^{+3.8}_{-3.9}\,\mathrm{km\,s^{-1}\,Mpc^{-1}}$. With systematics, we get $H_0 = 66.2^{+5.5}_{-5.6}\,\mathrm{km\,s^{-1}\,Mpc^{-1}}$. While the central value of our predicted H_0 is close to the estimates from Planck, DESI DR1, and DESI DR2, the associated uncertainty is notably larger.

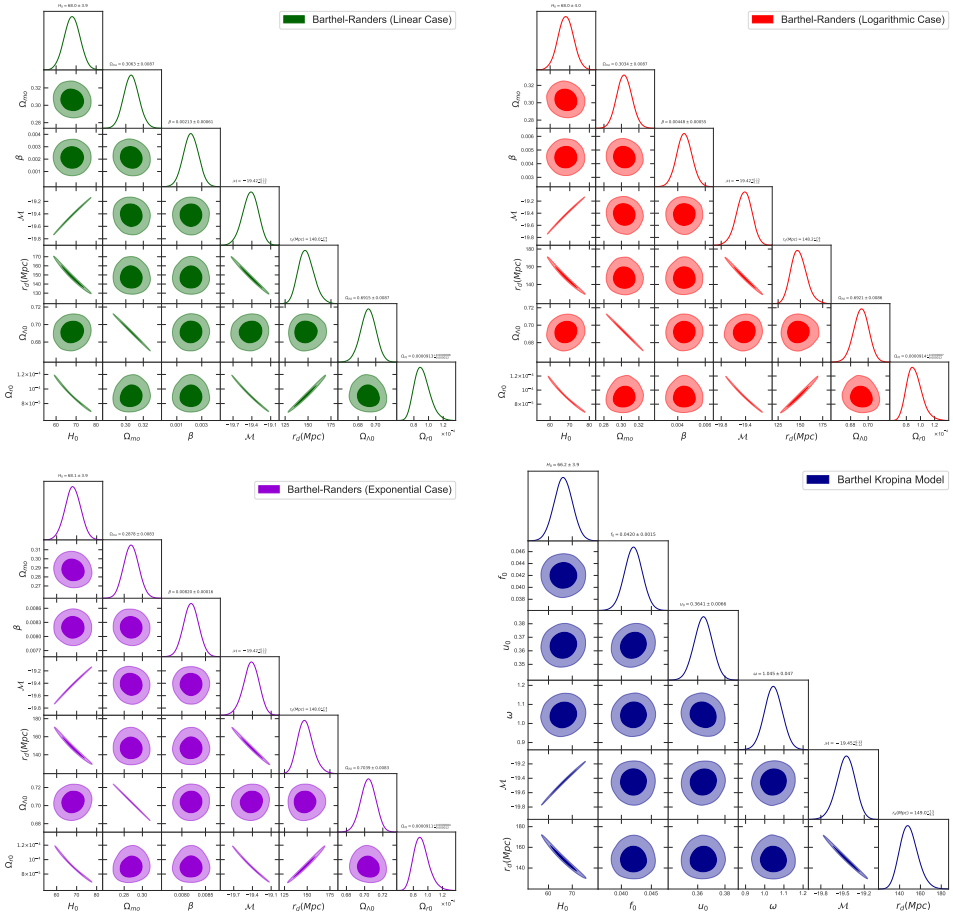


Figure 2. The figure shows the parameter constraints of the Barthel–Randers and Barthel–Kropina models using the CC + SNe Ia and BAO datasets together, and displaying both 1σ and 2σ confidence intervals. The contours show the correlations between these parameters, with marginalized probability distributions along the diagonal.

A similar trend is observed for r_d, where the predicted central values across all models are close to the Planck estimation, $r_d^{\text{Planck}} = (147.09 \pm 0.26)$ Mpc, although the associated uncertainty is also noticeably larger. The primary reason for the higher uncertainty is the inclusion of the full cosmic covariance matrix, which accounts for uncertainties in several factors, including the estimation of stellar metallicity, star formation history, the adopted initial mass function (IMF), the stellar library used, the stellar population synthesis model, and potential contributions from any residual young components in the galaxy spectra.

Table 2 presents the mean values at corresponding 68% confidence intervals for the model parameters of the Barthel–Randers models (linear, logarithmic, and exponential cases), as well as for the osculating Barthel–Kropina dark energy model. The predicted value of the present-day matter density parameter in the case of the ΛCDM model, as well as the linear case of the Barthel–Randers model, is lower than the Planck estimation, $\Omega_{m0}^{\text{Planck}} = 0.315 \pm 0.007$, and is closer to the values predicted by DESI DR1 and DESI DR2, $\Omega_{m0}^{\text{DESI DR1}} = 0.295 \pm 0.015$ and $\Omega_{m0}^{\text{DESI DR2}} = 0.2975 \pm 0.0086$.

Similarly, the predicted value of Ω_{m0} in the logarithmic case of the Barthel–Randers model is also in good agreement with the DESI DR1 and DR2 estimations. In contrast, the exponential case of the Barthel–Randers model predicts a matter density parameter that is lower than the values reported by both DESI DR1 and DR2. It is interesting to observe that the ΛCDM model, as well as the linear, logarithmic, and exponential cases of the Barthel–Randers model, predict a present-day dark energy density parameter, $\Omega_{\Lambda 0}$, that is greater than the value predicted by the Planck estimation: $\Omega_{\Lambda 0}^{\text{Planck}} = 0.685 \pm 0.007$.

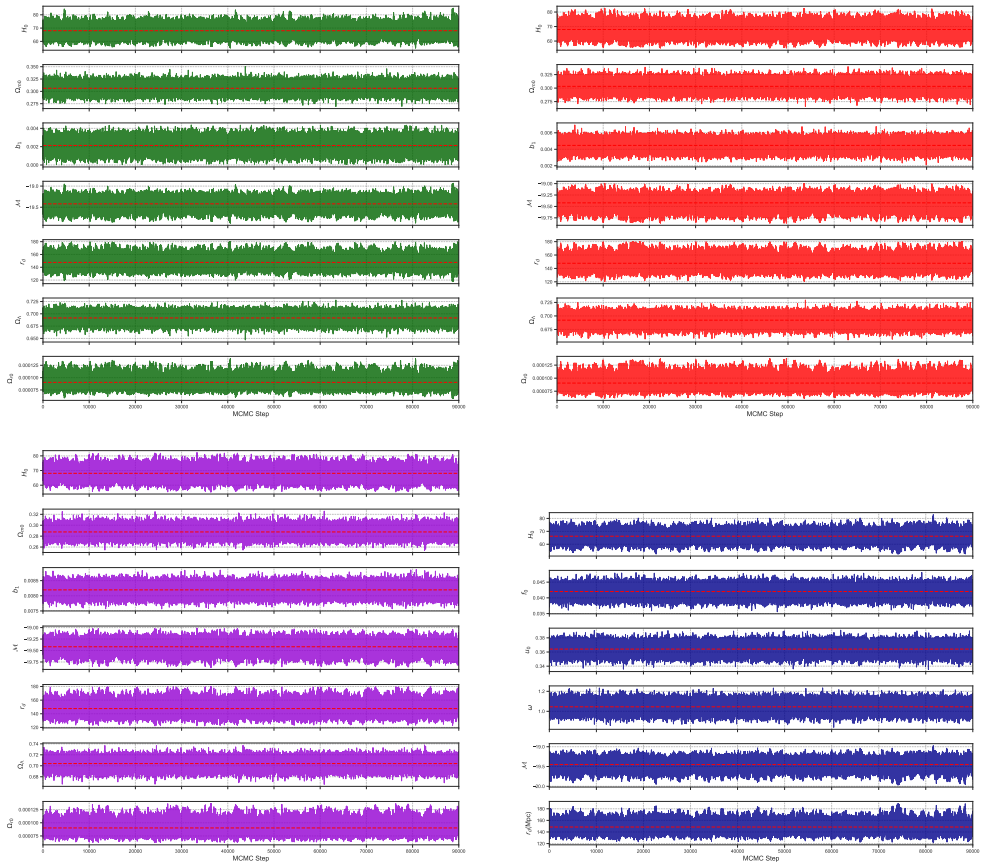


Figure 3. The figure illustrates the trace plots, which show the convergence behavior of the Markov chains for each parameter in the Barthel–Randers and Barthel–Kropina cosmological models.

Table 2. Summary of the mean values and 68% confidence intervals (1σ) for the parameters of the ΛCDM, Barthel–Randers, and Barthel–Kropina cosmological models.

Cosmological Models	Parameter	JOINT
ΛCDM Model	H_0	67.8 ± 3.7
	Ω_{m0}	0.3092 ± 0.0086
	$\mathcal{M}$	-19.43 ± 0.12
	r_d	148.5 ± 7.5
	$\Omega_{\Lambda 0}$	0.6908 ± 0.0086
BR (Linear Case)	H_0	68.1 ± 4.0
	Ω_{m0}	0.3064 ± 0.0087
	β	0.00213 ± 0.00061
	$\mathcal{M}$	-19.42 ± 0.12
	r_d	147.9 ± 7.6
	$\Omega_{\Lambda 0}$	0.6914 ± 0.0087
	Ω_{r0}	$(9.11 \pm 1.20) \times 10^{-5}$

Table 2. *Cont.*

Cosmological Models	Parameter	JOINT
BR (Logarithmic Case)	H_0	68.9 ± 3.9
	Ω_{m0}	0.3034 ± 0.0087
	β	0.00447 ± 0.00055
	$\mathcal{M}$	-19.42 ± 0.12
	r_d	148.1 ± 7.4
	$\Omega_{\Lambda 0}$	0.6921 ± 0.0086
	Ω_{r0}	$(9.13 \pm 1.20) \times 10^{-5}$
BR (Exponential Case)	H_0	68.2 ± 4.0
	Ω_{m0}	0.2878 ± 0.0083
	β	0.00820 ± 0.00016
	$\mathcal{M}$	-19.42 ± 0.12
	r_d	147.9 ± 7.4
	$\Omega_{\Lambda 0}$	0.7040 ± 0.0083
	Ω_{r0}	$(9.00 \pm 1.20) \times 10^{-5}$
Barthel–Kropina Model	H_0	66.2 ± 3.9
	f_0	0.0420 ± 0.0015
	u_0	0.3641 ± 0.0066
	ω	1.045 ± 0.047
	$\mathcal{M}$	-19.45 ± 0.12
	r_d	149.0 ± 7.5

6.2. Hubble Parameter, Hubble Residual, and BAO Distance Scale Results

Figure 4 shows the evolution of the Hubble function and the Hubble residuals for the linear, logarithmic, and exponential cases of the Barthel–Randers model, as well as the Barthel–Kropina model. These are compared with the predictions from the ΛCDM model and CC measurements. The left panel shows that at high redshift ($z > 0.7$), all the considered models deviate noticeably from the ΛCDM model. However, these deviations are not significant. At low redshift ($z < 0.7$), each model aligns closely with the ΛCDM predictions.

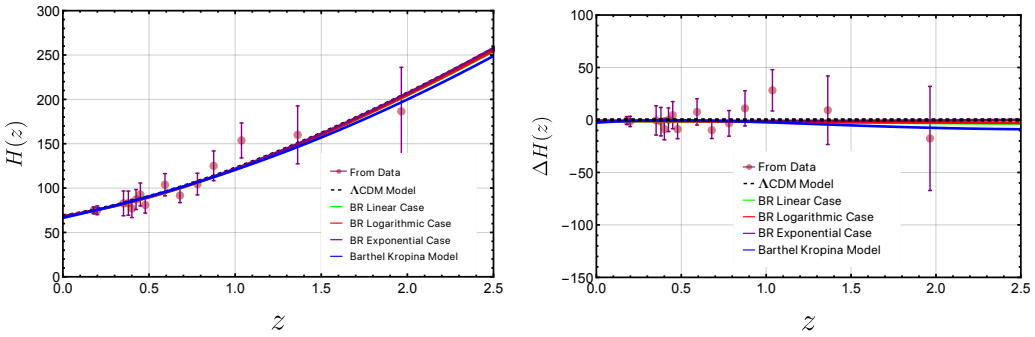


Figure 4. Comparison of the Barthel–Randers (linear, logarithmic, and exponential) and Barthel–Kropina models, with the ΛCDM model and CC measurements. The left panel shows the evolution of the Hubble parameter $H(z)$ using mean MCMC values. The right panel shows the Hubble residuals $\Delta H(z)$, indicating deviations from the standard model.

On the right plane, we can also observe similar behavior in the Hubble residual plots, where each model shows a slight deviation from the ΛCDM model at high redshift. However, at low redshift, all models exhibit behavior that closely matches the ΛCDM predictions. All considered models (Barthel–Randers variants and Barthel–Kropina) closely

follow ΛCDM at low redshifts, indicating consistency with current observations. Their mild deviations at higher redshifts ($z > 0.7$) suggest a potentially different early Universe expansion history, offering alternative insights that may help address cosmological tensions such as the Hubble tension.

Figure 5 shows the evolution of different BAO distance scales. All three Barthel–Randers variants exhibit minimal deviation in both the volume-averaged distance $D_V/(r_d z^{2/3})$ and the transverse distance measure $D_M/(zD_H)$, indicating strong alignment with cosmological observations. The logarithmic and exponential BR models closely match ΛCDM at low to intermediate redshifts ($z < 1.5$), though some discrepancies appear beyond $z \approx 1.5$, particularly with the exponential model diverging in the D_V observable range and both models showing reduced accuracy for high-redshift QSO and Ly-α data. The Barthel–Kropina model displays a distinct profile, with the $D_V/(r_d z^{2/3})$ curve generally below the ΛCDM prediction, especially in the mid-redshift range ($z \sim 0.5 - 1.2$). Despite this, it remains within observational error for $z < 1$. In terms of $D_M/(zD_H)$, the Barthel–Kropina model performs similarly to ΛCDM but shows more pronounced deviations in residuals, particularly around $z \sim 1$, indicating less precise modeling in this region.

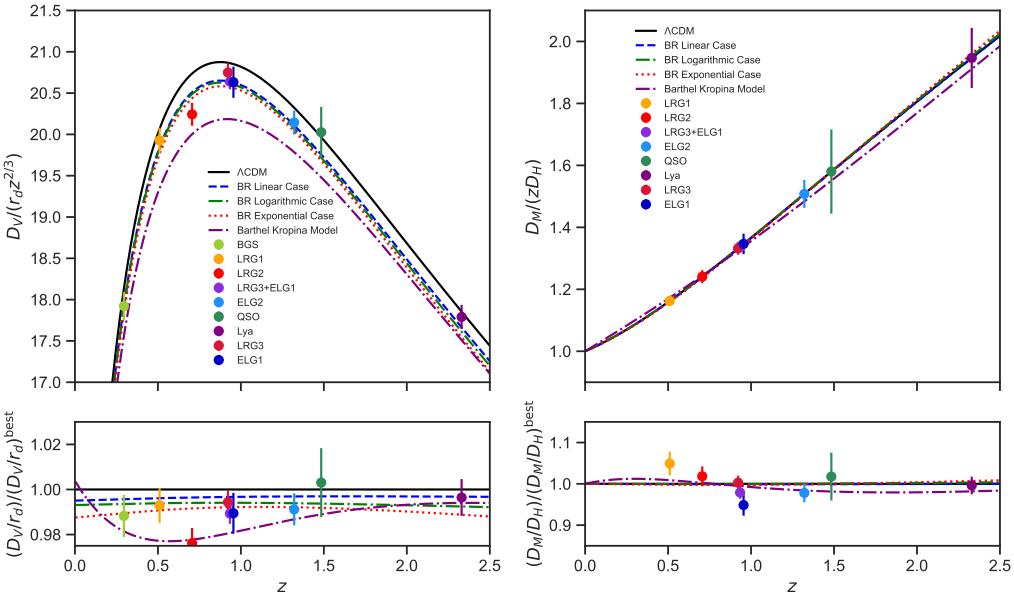


Figure 5. Comparison of the Barthel–Randers (linear, logarithmic, and exponential) and Barthel–Kropina models, with the ΛCDM model across various distance measures, with data from tracers such as LRG, QSO, and Lya. Measurement uncertainties are represented by error bars. In the left panel, the evolution of the ratio between the angle-averaged distance $D_V \equiv (zD_M^2 D_H)^{1/3}$ and the sound horizon at the baryon drag epoch, r_d, is shown. The right panel illustrates the ratio of transverse to line-of-sight comoving distances $FAP \equiv D_M/D_H$. To enhance clarity and compress the dynamic range, an arbitrary scaling of $z^{-2/3}$ has been applied to the left panel, and z^{-1} to the right. The bottom row presents the same models and data points as the top row, but now scaled as the ratio relative to the best-fit flat ΛCDM model predictions.

6.3. Cosmographic Results

Figure 6 shows the evolution of the cosmography parameters for the linear, logarithmic, and exponential cases of the Barthel–Randers model, along with the Barthel–Kropina model, compared to the ΛCDM model. The left panel shows the evolution of the deceleration parameter, $q(z)$.

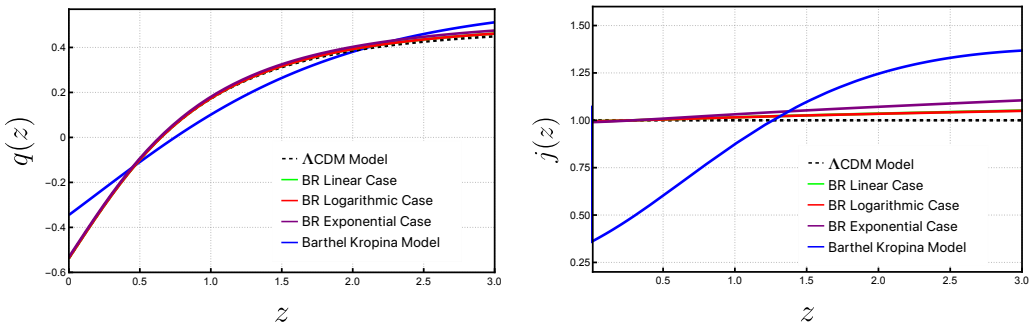


Figure 6. Evolution of the deceleration parameter $q(z)$ and jerk parameter $j(z)$ for the Barthel–Randers (linear, logarithmic, and exponential) and Barthel–Kropina models, and of the ΛCDM model. The left panel shows the evolution of $q(z)$ as a function of redshift, while the right panel presents $j(z)$, showing deviations from the ΛCDM value $j = 1$.

Notably, the Barthel–Kropina model exhibits a distinct evolution compared to both the standard ΛCDM model and the Barthel–Randers variants. At the present time ($z = 0$), all Barthel–Randers variants and ΛCDM predict a deceleration parameter of approximately $q_0 \approx -0.511$, while the Barthel–Kropina model predicts a less negative value of $q_0 \approx -0.366$. We also analyze an important cosmological feature: the transition redshift $z_{\rm tr}$.

For the ΛCDM model, the transition from decelerated to accelerated expansion occurs at $z_{\rm tr}^{\Lambda\rm CDM} \approx 0.623$. The Barthel–Randers variants exhibit slightly later transitions: $z_{\rm tr}^{\rm BR\ Linear} \approx 0.610$, $z_{\rm tr}^{\rm BR\ Logarithmic} \approx 0.607$, and $z_{\rm tr}^{\rm BR\ Exponential} \approx 0.606$.

In contrast, the Barthel–Kropina model shows a significantly earlier transition at $z_{\rm tr}^{\rm Barthel\text{-}Kropina} \approx 0.723$. While at high redshift, all models show deviations from the ΛCDM model in their evolution, these deviations are not significant. The right panel shows the evolution of the jerk parameter for each model. At the present time ($z = 0$), all variants of the Barthel–Randers models exhibit good agreement with the ΛCDM model. Although each variant predicts a slightly different value for the jerk parameter, these deviations are not significant. Moreover, the Barthel–Kropina model shows a substantial deviation from the other models, predicting a present-day jerk value of $j_0^{\rm Barthel\text{-}Kropina} \approx 0.448$.

At high redshift, all variants of the Barthel–Randers models, as well as the Barthel–Kropina model, deviate from the predictions of the ΛCDM model.

6.4. Statistical Results

Table 3 presents a comparative analysis of the linear case, logarithmic case, and exponential case of the Barthel–Randers model, as well as the Barthel–Kropina model, against the ΛCDM model, using several statistical metrics. The $\chi^2_{\rm tot,min}$ value for the ΛCDM model is 1780.94. The Barthel–Randers models (linear, logarithmic, and exponential cases) show similar total $\chi^2_{\rm tot,min}$ values ranging from 1781.22 to 1783.38, which are slightly higher than those of the ΛCDM model. The Barthel–Kropina model shows the lowest $\chi^2_{\rm tot,min}$ value of 1762.37. This indicates that, in terms of overall goodness of fit, the Barthel–Kropina model provides the best fit, while the Barthel–Randers models perform slightly worse than the ΛCDM model.

The $\chi^2_{\rm red}$ value provides insight into the goodness of fit adjusted for the number of data points and parameters in the model. The ΛCDM model has a $\chi^2_{\rm red}$ of 1.032, which is very close to the Barthel–Randers models, all of which have values slightly above 1.033. The lowest $\chi^2_{\rm red}$ value is from the Barthel–Kropina model (1.022), indicating that it is marginally the best in terms of adjusting for the complexity of the model and fitting the data well.

Table 3. Summary of $\chi^2_{\rm tot}$, $\chi^2_{\rm red}$, AIC, ΔAIC, BIC, ΔBIC, and p-value for the ΛCDM, Barthel–Randers, and Barthel–Kropina models.

Models	$\chi^2_{\rm tot}$	DoF	$\chi^2_{\rm red}$	AIC	ΔAIC	BIC	ΔBIC	p-Value
ΛCDM	1780.94	1725	1.032	1788.94	0	1810.76	0.170	0.167
BR (Linear Case)	1781.22	1724	1.033	1791.22	2.27	1818.49	7.74	0.164
BR (Logarithmic Case)	1781.60	1724	1.033	1791.60	2.65	1818.87	8.11	0.163
BR (Exponential Case)	1783.38	1724	1.034	1793.38	4.44	1820.65	9.89	0.155
Barthel–Kropina	1762.37	1723	1.022	1774.37	−14.57	1807.10	−3.65	0.249

The AIC is a measure of the relative quality of a model, accounting for both the goodness of fit and the number of parameters. The ΛCDM model has an AIC of 1788.94. The Barthel–Randers models (linear, logarithmic, and exponential) have AIC values around 1791.22, 1791.60, and 1793.38, which are higher by 2.27, 2.65, and 4.44, respectively, compared to the ΛCDM model, indicating a slightly worse balance between fit and model complexity. The Barthel–Kropina model has the lowest AIC value of 1774.37, which is 14.57 points lower than the ΛCDM model. According to the AIC, the Barthel–Kropina model provides the best balance between fit and complexity, while the Barthel–Randers models perform slightly worse than the ΛCDM model.

The BIC is another metric for model selection, similar to AIC but with a stronger penalty for the number of parameters. The ΛCDM model has a BIC of 1810.76, which is lower than the Barthel–Randers models but slightly higher than the Barthel–Kropina model. The Barthel–Randers models show BIC values between 1818.49 and 1820.65, with an increase of approximately 7.74 to 9.89 compared to the ΛCDM model. The Barthel–Kropina model has the lowest BIC of 1807.10, a decrease of 3.65 compared to the ΛCDM model. This suggests that the Barthel–Kropina model is the best according to the BIC criterion, while the Barthel–Randers models perform worse than the ΛCDM model.

The p-value indicates the statistical significance of the model in terms of explaining the data. The ΛCDM model has a p-value of 0.167, indicating that the model is statistically significant at a conventional level (i.e., it cannot be rejected at the 5% significance level). All the other models (Barthel–Randers linear, logarithmic, exponential, and Barthel–Kropina) have p-values ranging from 0.155 to 0.249, which are slightly higher or comparable, suggesting that none of the models can be rejected at the 5% significance level. The p-values imply that all models, including the base ΛCDM model, are statistically significant in explaining the data.

The Barthel–Kropina model outperforms the ΛCDM model in terms of goodness of fit, AIC, and BIC, offering a better balance between fit and model complexity. The Barthel–Randers models (linear, logarithmic, exponential), however, perform slightly worse than the ΛCDM model in this updated comparison.

Despite these improvements, all models, including the ΛCDM model, are statistically significant, with p-values indicating that none of them should be rejected. In terms of simplicity, however, the ΛCDM model remains the most straightforward and easiest to interpret. Therefore, while the Barthel–Kropina model appears to be the most favorable overall, the differences between the models are relatively small, and all offer comparable statistical significance.

7. Discussion and Final Remarks

One of the fundamental assumptions, and results, of present day physics is that the gravitational interaction can be successfully described only in geometric terms. However, which geometry can best describe gravity is still a matter of debate. The initial Riemannian framework of general relativity was extended to include geometries with non-metricity,

torsion, or both. While non-metricity naturally arises in the Finslerian setting, the torsional equivalent is not as immediate. Hence, formulating teleparallel theories in the Finslerian setting could be an interesting line of research. A mathematical study of teleparallel connections in Finsler geometry is presented in [192], and it has been shown that general teleparallel gravity could be obtained from Finsler geometry [193]. This opens up new possibilities of research: the exploration of $f(T)$ theories in the Finslerian setting, which, to the best of our knowledge, has not yet been achieved. While the discussion above is entirely classical, it is widely believed that quantum effects should become significant at the Planck scale. A central focus of quantum gravity phenomenology—aimed at identifying observable signatures of quantum gravity—is the study of modified dispersion relations [194,195]. The most well-known examples arise from frameworks such as doubly special relativity (DSR) [196,197] and the κ-Poincaré algebra [198]. Interestingly, the symmetries of doubly special relativity can be realized within the framework of Finsler geometry [199]. Therefore, further investigation into the connection between quantum gravity and Finsler geometry represents a promising direction for research.

In the present work, we have briefly reviewed some recent advances in the application of another geometric framework that could provide some insight into the understanding of the gravitational force, namely Finsler geometry, and its various particular cases. In Finsler geometry, instead of the point x of Riemann geometry, the metric depends also on an internal degree of freedom y, which is often physically interpreted as velocity. Hence, the y dependence is the essential characteristic of Finsler spaces, and the presence of this internal degrees of freedom opens some new perspective on the physical interpretation of the Finsler geometric theories. Thus, Finsler geometries are generally anisotropic and nonlocal, and these properties significantly enlarge the possibilities of the physical applications.

On the other hand, from a physical point of view it is natural to assume that in some specific physical processes, the internal vector y becomes a function of x. Such specific situations may occur if we interpret y as describing spacetime fluctuations, and we perform an averaging over it, according to the rule $\langle \phi(x) \rangle = \int \phi(x,y) f(y) d^4y$, where $f(y)$ is a specific distribution function of y [57]. Hence, Finsler geometry with $\widehat{g}(x) = g(x,y)|_{y=Y(x)}$ has a deep physical origin, which points towards interesting physical consequences. The averaging or the osculating process leads to a reduction of a Finsler geometry F to a corresponding Riemann geometry. The interpretation of the vector y as related to some quantum effects, like the vacuum fluctuation, is also supported by the fact that generally, in (α, β)-type gravitational theories, the matter energy–momentum tensor is not conserved. The most natural physical interpretation of this result is related to the possibility of particle production from the Finslerian vacuum in an expanding Universe, an effect that is also specific to quantum field theories in curved spacetimes [147–151]. Hence, Finslerian-type gravitational theories can offer a glimpse of the structure and classical limit of quantum field theories in Riemann geometries.

In our presentation, we have concentrated on a specific class of osculating geometries, the osculating (α, β) geometries, which have the remarkable property that their Barthel connection is the Levi–Civita connection. This property allows a significant simplification of the mathematical formalism, which becomes easily tractable by using the standard methods of Riemannian geometry. The osculating (α, β)-type theories can be interpreted as two metric theories. First, we have the Finsler metric function $F(\alpha, \beta)$, which generates its own metric, while α is a Riemannian metric given a priori. For cosmological applications, the FLRW metric can be adopted as the Riemann metric α, and we assume that this is the physical metric in which the real, observable gravitational processes take place. However, the Finsler metric $\widehat{g}(x) = g(x, Y(x))$ also has an important imprint on gravitation, since its presence induces new terms in the gravitational field equations. We have investigated the effects of

these new terms from a cosmological perspective only, by interpreting them as describing an effective dark energy that is responsible for the late acceleration of the Universe.

An important test of a cosmological model is represented by its consistency with the observations. We have used three observational datasets (Cosmic Chronometers, Type Ia Supernovae, Baryon Acoustic Oscillations) to perform a detailed analysis, and comparison of the Barthel–Randers, Barthel–Kropina and ΛCDM models. Generally, one can appreciate that all the considered models give a good description of the observational data, but important differences still appear between the various Finslerian approaches and the ΛCDM model. The differences appear, for example, in the prediction of the critical redshift z_{crit} at which the transition from deceleration to acceleration occurs, with the Barthel–Randers models predicting a value of z_{crit} of the order of $z_{crit} \approx 0.60$, while that in the Barthel–Kropina cosmology is $z_{crit} \approx 0.72$. Significant differences appear in the present values of the deceleration parameter $q(0)$, which in the Barthel–Kropina cosmology takes the value $q(0) \approx -0.37$, while in ΛCDM and Barthel–Randers models, it has the value $q(0) \approx -0.50$. Moreover, at redshifts $z > 3$, the predictions of all considered models show significant differences with respect to each other. Hence, cosmological observations at high redshift will give the possibility of discriminating between the various cosmological models based on modified gravity theory constructed with the help of Finsler (and other) geometries.

The main goal of the present review is to draw attention to the possibilities offered by Finsler geometry in the explanation of the cosmological phenomena, and to give a brief introduction to the existing results in a very specific and simple class of this very complex geometry. We have presented in some detail the generalized Friedmann cosmological equations, and the general theoretical framework in which cosmological models can be constructed. We would like to point out that from the point of view of calculations, the derivations of the field equations and of the evolution equations in these particular geometries are no more complicated than those in standard general relativity. This is related especially to the important fact that the connection in osculating-point Finsler geometries is, for the (α, β) metrics, the Barthel connection, which has the same mathematical form as the Levi–Civita connection. In our review, we have presented some basic theoretical tools that can be used for the further exploration of the applications of Finsler geometry in the description of gravitational phenomena.

Author Contributions: Conceptualization, S.V.S., R.H., S.S. and T.H.; methodology L.C., S.S. and S.V.S.; software A.B. and H.C.; review and editing T.H., L.C., A.B. and H.C. All authors have read and agreed to the published version of the manuscript.

Funding: The work of L.Cs. was supported by a grant of the Ministry of Research, Innovation and Digitization, CNCS/CCCDI-UEFISCDI, project number PN-IV-P8-8.1-PRE-HE-ORG-2023-0118, within PNCDI IV and Collegium Talentum Hungary. T. H. was supported by a grant from Collegium Talentum Hungary.

Data Availability Statement: The data underlying this article is already given with references during the analysis of this work.

Acknowledgments: We would like to thank the anonymous referees for comments and suggestions that helped to improve our manuscript.

Conflicts of Interest: The authors declare no conflicts of interest. The funders had no role in the design of the study; in the collection, analyses, or interpretation of data; in the writing of the manuscript; or in the decision to publish the results

Notes

[1] https://emcee.readthedocs.io/en/stable/ (accessed on 14 June 2025)
[2] https://getdist.readthedocs.io/en/latest/plot_gallery.html (accessed on 14 June 2025)
[3] https://gitlab.com/mmoresco/CCcovariance (accessed on 14 June 2025)
[4] https://github.com/CobayaSampler/bao_data (accessed on 14 June 2025)
[5] https://github.com/CobayaSampler/bao_data/blob/master/desi_bao_dr2/desi_gaussian_bao_ALL_GCcomb_cov.txt (accessed on 14 June 2025)

References

1. Weyl, H. Gravitation und Elektrizität. In *Sitzungsberichte der Königlich Preussischen Akademie der Wissenschaften zu Berlin*, 1918th ed.; Königlich Preussische Akademie: Berlin, Germany, 1918; pp. 465–480.
2. Weyl, H. *Space, Time, Matter*; Dover Publications: New York, NY, USA, 1952.
3. Finsler, P. Über Kurven und Flächen in Allgemeinen Räumen. Ph.D. Thesis, University of Göttingen, Göttingen, Germany, 1918.
4. Einstein, A. Die Feldgleichungen der Gravitation. In *Sitzungsberichte der Königlich Preussischen Akademie der Wissenschaften zu Berlin*, 1915th ed.; Königlich Preussische Akademie: Berlin, Germany, 1915; pp. 844–847.
5. Einstein, A. Die Grundlage der allgemeinen Relativitätstheorie. *Ann. Phys.* **1916**, *49*, 769–822. [CrossRef]
6. Hilbert, D. Die Grundlagen der Physik. *Nachrichten Ges. Wiss. Göttingen Math.-Phys. KI.* **1915**, *1915*, 395–408.
7. Scholz, E. The Unexpected Resurgence of Weyl Geometry in late 20th-Century Physics. In *Beyond Einstein: Perspectives on Geometry, Gravitation, and Cosmology in the Twentieth Century*; Rowe, D.E., Sauer, T., Walter, S.A., Eds.; Springer: New York, NY, USA, 2018; pp. 261–360.
8. Riemann, B. Über die Hypothesen, welche der Geometrie zu Grunde liegen. *Abh. KöNiglichen Ges. Wiss. GöTtingen* **1868**, *13*, 133–150.
9. Chern, S.S. Finsler Geometry Is Just Riemannian Geometry without the Quadratic Restriction. *Not. Am. Math. Soc.* **1996**, *43*, 959–963.
10. Rund, H. *The Differential Geometry of Finsler Spaces*; Springer: Berlin, Germany, 1959.
11. Bejancu, A. *Finsler Geometry and Applications*; Ellis Horwood: New York, NY, USA, 1990.
12. Bao, D.; Chern, S.-S.; Shen, Z. *An Introduction to Riemann-Finsler Geometry*; Springer: New York, NY, USA, 2000.
13. Shen, Y.-B.; Shen, Z. *Introduction to Modern Finsler Geometry*; World Scientific: Singapore, 2016.
14. Will, C.M. The Confrontation between General Relativity and Experiment. *Living Rev. Relativ.* **2014**, *17*, 4. [CrossRef]
15. Abbott, B.P. et al. [LIGO Scientific Collaboration and Virgo Collaboration] Observation of Gravitational Waves from a Binary Black Hole Merger. *Phys. Rev. Lett.* **2016**, *116*, 061102.
16. Abbott, R. et al. [LIGO Scientific Collaboration and Virgo Collaboration] GW190814: Gravitational Waves from the Coalescence of a 23 Solar Mass Black Hole with a 2.6 Solar Mass Compact Object. *Astrophys. J. Lett.* **2020**, *896*, L44. [CrossRef]
17. Cartan, É. Sur les variétés à connexion affine et la théorie de la relativité généralisée. *Ann. L'École Norm. Supérieure* **1924**, *41*, 1–25. [CrossRef]
18. Cartan, É. Sur les variétés à connexion affine et la théorie de la relativité généralisée. *Ann. L'École Norm. Supérieure* **1925**, *42*, 17–88. [CrossRef]
19. Weitzenböck, R. *Invariantentheorie*; Noordhoff: Groningen, The Netherlands, 1923.
20. Ehlers, J.; Pirani, F.A.E.; Schild, A. The Geometry of Free Fall and Light Propagation. *Gen. Relativ. Gravit.* **2012**, *44*, 1587. [CrossRef]
21. Linnemann, N.; Read, J. Constructive Axiomatics in Spacetime Physics Part I: Walkthrough to the Ehlers-Pirani-Schild Axiomatisation. *arXiv* **2021**, arXiv:2112.14063.
22. Adlam, E.; Linnemann, N.; Read, J. Constructive Axiomatics in Spacetime Physics Part II: Constructive Axiomatics in Context. *arXiv* **2022**, arXiv:2211.05672.
23. Adlam, E.; Linnemann, N.; Read, J. Constructive Axiomatics in Spacetime Physics Part III: A Constructive Axiomatic Approach to Quantum Spacetime. *arXiv* **2022**, arXiv:2208.07249.
24. Pfeifer, C. Finsler Spacetime Geometry in Physics. *Int. J. Geom. Methods Mod. Phys.* **2019**, *16* (Suppl. S2), 1941004. [CrossRef]
25. Randers, G. On an Asymmetrical Metric in the Four-Space of General Relativity. *Phys. Rev.* **1941**, *59*, 195. [CrossRef]
26. Ingarden, R. On the Geometrically Absolute Optical Representation in the Electron Microscope. *Trav. Société Sci. Lettres WrocłAw Série B* **1957**, *45*, 3.
27. Miron, R. The Geometry of Ingarden Spaces. *Rep. Math. Phys.* **2004**, *54*, 131. [CrossRef]
28. Tavernelli, I. On the Geometrization of Quantum Mechanics. *Ann. Phys.* **2016**, *371*, 239. [CrossRef]
29. Tavernelli, I. On the Self-Interference in Electron Scattering: Copenhagen, Bohmian and Geometrical Interpretations of Quantum Mechanics. *Ann. Phys.* **2018**, *393*, 447. [CrossRef]

30. Liang, S.-D.; Sabau, S.V.; Harko, T. Finslerian Geometrization of Quantum Mechanics in the Hydrodynamical Representation. *Phys. Rev. D* **2019**, *100*, 105012. [CrossRef]
31. Tavernelli, I. Gravitational Quantum Dynamics: A Geometrical Perspective. *Found. Phys.* **2021**, *51*, 46. [CrossRef]
32. Hohmann, M.; Pfeifer, C.; Voicu, N. The Kinetic Gas Universe. *Eur. Phys. J. C* **2020**, *80*, 809. [CrossRef]
33. Pfeifer, C.; Voicu, N.; Friedl-Szász, A.; Popovici-Popescu, E. From Kinetic Gases to an Exponentially Expanding Universe. *arXiv* **2025**, arXiv:2504.08062.
34. Rätzel, D.; Rivera, S.; Schuller, F.P. Geometry of Physical Dispersion Relations. *Phys. Rev. D* **2011**, *83*, 044047. [CrossRef]
35. Duval, C. Finsler Spinoptics. *Commun. Math. Phys.* **2008**, *283*, 701–727. [CrossRef]
36. Schreck, M. Classical Lagrangians and Finsler Structures for the Nonminimal Fermion Sector of the Standard-Model Extension. *Phys. Rev. D* **2016**, *93*, 105017. [CrossRef]
37. Edwards, B.R.; Kostelecký, V.A. Riemann–Finsler Geometry and Lorentz-Violating Scalar Fields. *Phys. Lett. B* **2018**, *786*, 319–326. [CrossRef]
38. Horváth, J.I. A Geometrical Model for the Unified Theory of Physical Fields. *Phys. Rev.* **1950**, *80*, 901. [CrossRef]
39. Horváth, J.I.; Moór, A. Entwicklung einer einheitlichen Feldtheorie begründet auf die Finslersche Geometrie. *Z. Für Phys.* **1952**, *131*, 548. [CrossRef]
40. Takano, Y. Gravitational Field in Finsler Spaces. *Lett. Nuovo Cimento* **1974**, *10*, 747. [CrossRef]
41. Takano, Y. Variation Principle in Finsler Spaces. *Lett. Nuovo Cimento* **1974**, *11*, 486. [CrossRef]
42. Asanov, G.S. A Finslerian Extension of General Relativity. *Found. Phys.* **1981**, *11*, 137. [CrossRef]
43. Asanov, G.S. *Finsler Geometry, Relativity and Gauge Theories*; D. Reidel: Dordrecht, The Netherlands, 1985.
44. Asanov, G.S. Finslerian Solution for Static Spherically Symmetric Gravitational Field. *Fortschritte Phys.* **1991**, *39*, 185. [CrossRef]
45. Asanov, G.S. Finslerian Extension of Schwarzschild Metric. *Fortschritte Phys.* **1992**, *40*, 667. [CrossRef]
46. Malligawad, M.; Narasimhamurthy, S.K.; Nekouee, Z.; Yashwanth, B.R. Shadow analysis and light deflection in charged Finslerian Kiselev black holes under spherical accretion. *Ann. Phys.* **2025**, *477*, 70005. [CrossRef]
47. Nekouee, Z.; Narasimhamurthy, S.K.; Yashwanth, B.R.; Sanjay, T. Exploring null geodesic of Finslerian hairy black hole. *Class. Quantum Gravity* **2025**, *42*, 045002. [CrossRef]
48. Yashwanth, B.R.; Narasimhamurthy, S.K.; Nekouee, Z.; Malligawad, M. Geodesics of Finsler Hayward Black Hole Surrounded by Quintessence. *Eur. Phys. J. C* **2025**, *84*, 1276 [CrossRef]
49. Malligawad, M.; Narasimhamurthy, S.K.; Nekouee, Z. Exploring the quintessential influence on shadows of black holes in Finsler-Hayward geometry. *Phys. Lett. B* **2024**, *856*, 138963. [CrossRef]
50. Yashwanth, B.R.; Narasimhamurthy, S.K.; Nekouee, Z. Generalized Finslerian Wormhole Models in $f(R,T)$ Gravity. *Particles* **2024**, *7*, 747–767. [CrossRef]
51. Nekouee, Z.; Narasimhamurthy, S.K.; Pacif, S.K.J. Black Hole Solutions with Constant Ricci Scalar in a Model of Finsler Gravity. *J. Cosmol. Astropart. Phys.* **2024**, *2024*, 061. [CrossRef]
52. Malligawad, M.; Narasimhamurthy, S.K.; Nekouee, Z.; Kumbar, M.Y. Finslerian wormhole solution in the framework of modified gravity. *Phys. Scr.* **2024**, *99*, 045206. [CrossRef]
53. Sanjay, T.; Narasimhamurthy, S.K.; Nekouee, Z.; Manjunatha, H.M. Traversable wormhole model in Finslerian geometry. *Pramana—J. Phys.* **2024**, *98*, 16. [CrossRef]
54. Nekouee, Z.; Narasimhamurthy, S.K. Thermodynamic product formulae for Finslerian Kiselev black hole. *Eur. Phys. J. C* **2023**, *83*, 723. [CrossRef]
55. Manjunath, M.; Narasimhamurthy, S.K.; Nekouee, Z.; Yashwanth, B.R.; Mallikarjun, Y.K. Finsler geometry insights into wormhole traversability and physical properties. *Indian J. Phys.* **2025**. [CrossRef]
56. Miron, R.; Anastasiei, M. *Vector Bundles, Lagrange Spaces, and Applications to the Theory of Relativity*; Editura Academiei Române: Bucharest, Romania, 1987. (In Romanian)
57. Ikeda, S. *Advanced Studies in Applied Geometry*; Seizansha: Sagamihara, Japan, 1995.
58. Rutz, S.F. A Finsler Generalisation of Einstein's Vacuum Field Equations. *Gen. Relativ. Gravit.* **1993**, *25*, 1139. [CrossRef]
59. Li, X.; Chang, Z. Towards a gravitation theory in Berwald–Finsler space. *Chin. Phys. C* **2010**, *34*, 28.
60. Hohmann, M.; Pfeifer, C.; Voicu, N. Finsler Gravity Action from Variational Completion. *Phys. Rev. D* **2019**, *100*, 064035. [CrossRef]
61. Riess, A.G. et al. [Supernova Search Team] Observational Evidence from Supernovae for an Accelerating Universe and a Cosmological Constant. *Astron. J.* **1998**, *116*, 1009. [CrossRef]
62. Perlmutter, S. et al. [Supernova Cosmology Project] Measurements of Ω and Λ from 42 High-Redshift Supernovae. *Astrophys. J.* **1999**, *517*, 565. [CrossRef]
63. Knop, R.A.; Aldering, G.; Amanullah, R.; Astier, P.; Blanc, G.; Burns, M.S.; Conley, A.; Deustua, S.E.; Doi, M.; Ellis, R.; et al. New Constraints on Ω_M, Ω_Λ, and w from an Independent Set of Eleven High-Redshift Supernovae Observed with HST. *Astrophys. J.* **2003**, *598*, 102. [CrossRef]

64. Amanullah, R.; Lidman, C.; Rubin, D.; Aldering, G.; Astier, P.; Barbary, K.; Burns, M.S.; Conley, A.; Dawson, K.S.; Deustua, S.E.; et al. Spectra and Hubble space telescope Light Curves of Six Type Ia Supernovae at $0.511 < z < 1.12$ and the Union2 Compilation. *Astrophys. J.* **2010**, *716*, 712.
65. Weinberg, D.H.; Mortonson, M.J.; Eisenstein, D.J.; Hirata, C.; Riess, A.G.; Rozo, E. Observational Probes of Cosmic Acceleration. *Phys. Rep.* **2013**, *530*, 87.
66. Einstein, A. *Kosmologische Betrachtungen zur Allgemeinen Relativitätstheorie*; Sitzungsberichte der Königlich Preußischen Akademie der Wissenschaften: Berlin, Germany, 1917.
67. Weinberg, S. The Cosmological Constant Problem. *Rev. Mod. Phys.* **1989**, *61*, 1. [CrossRef]
68. Salucci, P.; Turini, N.; Di Paolo, C. Paradigms and Scenarios for the Dark Matter Phenomenon. *Universe* **2020**, *6*, 118. [CrossRef]
69. Alam, S. et al. [BOSS Collaboration] The Clustering of Galaxies in the Completed SDSS-III Baryon Oscillation Spectroscopic Survey: Cosmological Analysis of the DR12 Galaxy Sample. *Mon. Not. R. Astron. Soc.* **2017**, *470*, 2617. [CrossRef]
70. Abbott, T.M.C. et al. [DES Collaboration] Dark Energy Survey Year 1 Results: Cosmological Constraints from Galaxy Clustering and Weak Lensing. *Phys. Rev. D* **2018**, *98*, 043526. [CrossRef]
71. Tanabashi, M. et al. [Particle Data Group] Review of Particle Physics. *Phys. Rev. D* **2018**, *98*, 030001. [CrossRef]
72. Aghanim, N. et al. [Planck Collaboration] Planck 2018 Results. VI. Cosmological Parameters. *Astron. Astrophys.* **2020**, *641*, A6. [CrossRef]
73. Martel, H.; Shapiro, P.R.; Weinberg, S. Likely Values of the Cosmological Constant. *Astrophys. J.* **1998**, *492*, 29. [CrossRef]
74. Weinberg, S. The Cosmological Constant Problems. In *Sources and Detection of Dark Matter and Dark Energy in the Universe*; Cline, D.B., Ed.; Springer: Berlin, Germany, 2001; p. 18.
75. Lake, M.J. Why space could be quantised on a different scale to matter. *SciPost Phys. Proc.* **2021**, *4*, 014. [CrossRef]
76. Riess, A.G.; Casertano, S.; Yuan, W.; Macri, L.M.; Scolnic, D. Large Magellanic Cloud Cepheid Standards Provide Foundation for the Determination of the Hubble Constant and Stronger Evidence for Physics Beyond LCDM. *Astrophys. J.* **2019**, *876*, 85. [CrossRef]
77. Huang, C.D.; Riess, A.G.; Yuan, W.; Macri, L.M.; Zakamska, N.L.; Casertano, S.; Whitelock, P.A.; Hoffmann, S.L.; Filippenko, A.V.; Scolnic, D. Hubble Space Telescope Observations of Mira Variables in the SN Ia Host NGC 1559: An Alternative Candle to Measure the Hubble Constant. *Astrophys. J.* **2020**, *889*, 5. [CrossRef]
78. Pesce, D.W.; Braatz, J.A.; Reid, M.J.; Riess, A.G.; Scolnic, D.; Condon, J.J.; Gao, F.; Henkel, C.; Impellizzeri, C.M.V.; Kuo, C.Y.; et al. The Megamaser Cosmology Project. XIII. Combined Hubble Constant Constraints. *Astrophys. J. Lett.* **2020**, *891*, L1. [CrossRef]
79. Harko, T.; Lobo, F.S.N. Beyond Einstein's General Relativity: Hybrid Metric-Palatini Gravity and Curvature-Matter Couplings. *Int. J. Mod. Phys. D* **2020**, *29*, 2030008. [CrossRef]
80. Haghani, Z.; Harko, T.; Sepangi, H.R.; Shahidi, S. Weyl-Cartan-Weitzenböck Gravity as a Generalization of Teleparallel Gravity. *J. Cosmol. Astropart. Phys.* **2012**, *10*, 061. [CrossRef]
81. Haghani, Z.; Harko, T.; Sepangi, H.R.; Shahidi, S. Weyl-Cartan-Weitzenböck Gravity through Lagrange Multiplier. *Phys. Rev. D* **2013**, *88*, 044024. [CrossRef]
82. Nester, J.M.; Yo, H.-J. Symmetric Teleparallel General Relativity. *Chin. J. Phys.* **1999**, *37*, 113.
83. Beltrán Jiménez, J.; Heisenberg, L.; Koivisto, T. Coincident General Relativity. *Phys. Rev. D* **2018**, *98*, 044048. [CrossRef]
84. D'Agostino, R.; Luongo, O. Growth of Matter Perturbations in Nonminimal Teleparallel Dark Energy. *Phys. Rev. D* **2018**, *98*, 124013. [CrossRef]
85. Fontanini, M.; Huguet, E.; Le Delliou, M. Teleparallel gravity equivalent of general relativity as a gauge theory: Translation or Cartan connection? *Phys. Rev. D* **2019**, *99*, 064006. [CrossRef]
86. Koivisto, T.; Tsimperis, G. The Spectrum of Teleparallel Gravity. *Universe* **2019**, *5*, 80. [CrossRef]
87. Pereira, J.G.; Obukhov, Y.N. Gauge Structure of Teleparallel Gravity. *Universe* **2019**, *5*, 139. [CrossRef]
88. Blixt, D.; Hohmann, M.; Pfeifer, C. On the Gauge Fixing in the Hamiltonian Analysis of General Teleparallel Theories. *Universe* **2019**, *5*, 143. [CrossRef]
89. Coley, A.A.; van den Hoogen, R.J.; McNutt, D.D. Symmetry and Equivalence in Teleparallel Gravity. *J. Math. Phys.* **2020**, *61*, 072503. [CrossRef]
90. Haghani, Z.; Khosravi, N.; Shahidi, S. The Weyl–Cartan Gauss–Bonnet Gravity. *Class. Quantum Gravity* **2015**, *32*, 215016. [CrossRef]
91. Sotiriou, T.P.; Faraoni, V. f(R) Theories of Gravity. *Rev. Mod. Phys.* **2010**, *82*, 451. [CrossRef]
92. De Felice, A.; Tsujikawa, S. f(R) Theories. *Living Rev. Relativ.* **2010**, *13*, 3. [CrossRef]
93. Cai, Y.F.; Capozziello, S.; De Laurentis, M.; Saridakis, E.N. f(T) Teleparallel Gravity and Cosmology. *Rep. Prog. Phys.* **2016**, *79*, 106901. [CrossRef]
94. Nojiri, S.; Odintsov, S.D.; Oikonomou, V.K. Modified Gravity Theories on a Nutshell: Inflation, Bounce and Late-Time Evolution. *Phys. Rep.* **2017**, *692*, 1. [CrossRef]

95. Odintsov, S.D.; Oikonomou, V.K.; Giannakoudi, I.; Fronimos, F.P.; Lymperiadou, E.C. Recent Advances in Inflation. *Symmetry* **2023**, *15*, 1701. [CrossRef]
96. Basilakos, S.; Stavrinos, P. Cosmological Equivalence between the Finsler–Randers spacetime and the DGP Gravity Model. *Phys. Rev. D* **2013**, *87*, 043506. [CrossRef]
97. Exirifard, Q. Randers geometry as MOND/dark matter. *J. Cosmol. Astropart. Phys.* **2015**, *11*, 026. [CrossRef]
98. Silva, J.E.G.; Maluf, R.V.; Almeida, C.A.S. A nonlinear dynamics for the scalar field in Randers spacetime. *Phys. Lett. B* **2017**, *766*, 263. [CrossRef]
99. Papagiannopoulos, G.; Basilakos, S.; Paliathanasis, A.; Savvidou, S.; Stavrinos, P.C. Finsler–Randers cosmology: Dynamical analysis and growth of matter perturbations. *Class. Quantum Gravity* **2017**, *34*, 225008. [CrossRef]
100. Papagiannopoulos, G.; Basilakos, S.; Paliathanasis, A.; Pan, S.; Stavrinos, P. Dynamics in varying vacuum Finsler–Randers cosmology. *Eur. Phys. J. C* **2020**, *80*, 816. [CrossRef]
101. Raushan, R.; Chaubey, S. Finsler–Randers cosmology in the framework of a particle creation mechanism: A dynamical systems perspective. *Eur. Phys. J. Plus* **2020**, *135*, 228. [CrossRef]
102. Triantafyllopoulos, A.; Basilakos, S.; Kapsabelis, E.; Stavrinos, P.C. Schwarzschild-like solutions in Finsler-Randers gravity. *Eur. Phys. J. C* **2020**, *80*, 1200. [CrossRef]
103. Kapsabelis, E.; Triantafyllopoulos, A.; Basilakos, S.; Stavrinos, P.C. Applications of the Schwarzschild-Finsler-Randers model. *Eur. Phys. J. C* **2021**, *81*, 990. [CrossRef]
104. Kapsabelis, E.; Kevrekidis, P.G.; Stavrinos, P.C.; Triantafyllopoulos, A. Schwarzschild–Finsler–Randers spacetime: Geodesics, dynamical analysis and deflection angle. *Eur. Phys. J. C* **2022**, *82*, 1098. [CrossRef]
105. Nekouee, Z.; Narasimhamurthy, S.K.; Manjunatha, H.M.; Srivastava, S.K. Finsler–Randers model for anisotropic constant-roll inflation. *Eur. Phys. J. Plus* **2022**, *137*, 1388. [CrossRef]
106. Feng, W.; Yang, W.; Jiang, B.; Wang, Y.; Han, T.; Wu, Y. Theoretical analysis on the Barrow holographic dark energy in the Finsler–Randers cosmology. *Int. J. Mod. Phys. D* **2023**, *32*, 2350029. [CrossRef]
107. Das, P.D.; Debnath, U. Possible existence of traversable wormhole in Finsler–Randers geometry. *Eur. Phys. J. C* **2023**, *83*, 821. [CrossRef]
108. Triantafyllopoulos, A.; Kapsabelis, E.; Stavrinos, P.C. Raychaudhuri Equations, Tidal Forces, and the Weak-Field Limit in Schwarzshild–Finsler–Randers Spacetime. *Universe* **2024**, *10*, 26. [CrossRef]
109. Kapsabelis, E.; Saridakis, E.N.; Stavrinos, P.C. Finsler–Randers–Sasaki gravity and cosmology. *Eur. Phys. J. C* **2024**, *84*, 538. [CrossRef]
110. Praveen, J.; Narasimhamurthy, S.K.; Yashwanth, B.R. Exploring compact stellar structures in Finsler–Randers geometry with the Barthel connection. *Eur. Phys. J. C* **2024**, *84*, 597. [CrossRef]
111. r Liu, J.; Wang, R.; Gao, F. Nonlinear Dynamics in Variable-Vacuum Finsler–Randers Cosmology with Triple Interacting Fluids. *Universe* **2024**, *10*, 302. [CrossRef]
112. Nekouee, Z.; Narasimhamurthy, S.K.; Pourhassan, B.; Pacif, S.K.J. A phenomenological approach to the dark energy models in the Finsler–Randers framework. *Ann. Phys.* **2024**, *470*, 169787. [CrossRef]
113. Nekouee, Z.; Chaudhary, H.; Narasimhamurthy, S.K.; Pacif, S.K.J.; Malligawad, M. Cosmological tests of the dark energy models in Finsler-Randers Space-time. *J. High Energy Astrophys.* **2024**, *44*, 19. [CrossRef]
114. Praveen, J.; Narasimhamurthy, S.K. Matter bounce cosmology within Finsler-Randers geometry: A comprehensive study of anisotropic influences. *J. High Energy Astrophys.* **2024**, *44*, 300. [CrossRef]
115. Yashwanth, B.R.; Narasimhamurthy, S.K.; Praveen, J.; Malligawad, M. The influence of density models on wormhole formation in Finsler–Barthel–Randers geometry. *Eur. Phys. J. C* **2024**, *84*, 1272. [CrossRef]
116. Praveen, J.; Narasimhamurthy, S.K. The role of Finsler-Randers geometry in shaping anisotropic metrics and thermodynamic properties in black holes theory. *New Astron.* **2025**, *119*, 102404. [CrossRef]
117. Ikeda, S.; Saridakis, E.N.; Stavrinos, P.C.; Triantafyllopoulos, A. Cosmology of Lorentz Fiber-Bundle Induced Scalar-Tensor Theories. *Phys. Rev. D* **2019**, *100*, 124035. [CrossRef]
118. Fuster, A.; Pabst, C.; Pfeifer, C. Berwald Spacetimes and Very Special Relativity. *Phys. Rev. D* **2018**, *98*, 084062. [CrossRef]
119. Hohmann, M.; Pfeifer, C.; Voicu, N. Cosmological Finsler Spacetimes. *Universe* **2020**, *6*, 65. [CrossRef]
120. Hama, R.; Harko, T.; Sabau, S.V.; Shahidi, S. Cosmological Evolution and Dark Energy in Osculating Barthel–Randers Geometry. *Eur. Phys. J. C* **2021**, *81*, 742. [CrossRef]
121. Hama, R.; Rattanasak, R.; Harko, T.; Sabau, S.V. Dark Energy and Accelerating Cosmological Evolution from Osculating Barthel–Kropina Geometry. *Eur. Phys. J. C* **2022**, *82*, 385. [CrossRef]
122. Bouali, A.; Chaudhary, H.; Hama, R.; Harko, T.; Sabau, S.V.; San Martín, M. Cosmological Tests of the Osculating Barthel–Kropina Dark Energy Model. *Eur. Phys. J. C* **2023**, *83*, 121. [CrossRef]
123. Hama, R.; Harko, T.; Sabau, S.V. Conformal Gravitational Theories in Barthel–Kropina-Type Finslerian Geometry and Their Cosmological Implications. *Eur. Phys. J. C* **2023**, *83*, 1030. [CrossRef]

124. Tavakol, R.K.; Van den Bergh, N. Finsler Spaces and the Underlying Geometry of spacetime. *Phys. Lett. A* **1985**, *112*, 23. [CrossRef]
125. Tavakol, R.K. Geometry of Spacetime and Finsler Geometry. *Int. J. Mod. Phys. A* **2009**, *24*, 1678. [CrossRef]
126. Miron, R.; Hrimiuc, D.; Shimada, H.; Sabau, S.V. *The Geometry of Hamilton and Lagrange Spaces*; Kluwer Academic Publishers: Dordrecht, The Netherlands, 2001.
127. Javaloyes, M.A.; Sánchez, M. On the Definition and Examples of Finsler Metrics. *Ann. Sc. Norm. Super. Pisa Cl. Sci.* **2014**, *13*, 813. [CrossRef] [PubMed]
128. Yoshikawa, R.; Sabau, S.V. Kropina Metrics and Zermelo Navigation on Riemannian Manifolds. *Geom. Dedicata* **2014**, *171*, 119. [CrossRef]
129. Kropina, V.K. On Projective Finsler Spaces with a Metric of Special Form. *Nauchnye Dokl. Vyss. Shkoly Fiz.-Mat. Nauk.* **1959**, *2*, 38.
130. Kropina, V.K. On projective two-dimensional Finsler spaces with a special metric. *Trudy Sem. Vektor. Tenzor. Anal* **1961**, *11*, 277–292.
131. Matsumoto, M. On C-Reducible Finsler Spaces. *Tensor, New Ser.* **1972**, *24*, 29–37.
132. Matsumoto, M. Theory of Finsler Spaces with (α, β)-Metric. *Rep. Math. Phys.* **1992**, *31*, 43–83. [CrossRef]
133. Bácsó, S.; Cheng, X.; Shen, Z. Curvature Properties of (α, β)-Metrics. *Adv. Stud. Pure Math.* **2007**, *48*, 73–110.
134. Antonelli, P.L.; Ingarden, R.S.; Matsumoto, M. *The Theory of Sprays and Finsler Spaces with Applications in Physics and Biology*; Kluwer Academic Publishers: Dordrecht, The Netherlands, 1993.
135. Yoshikawa, R.; Sabau, S.V. Some remarks on the geometry of Kropina spaces. *Publ. Math. Debrecen* **2014**, *84*, 483–496. [CrossRef]
136. Sabau, S.V.; Shibuya, K.; Yoshikawa, R. Geodesics on Strong Kropina Manifolds. *Eur. J. Math.* **2017**, *3*, 1172–1224. [CrossRef]
137. Heefer, S.; Pfeifer, C.; van Voorthuizen, J.; Fuster, A. On the Metrizability of m-Kropina Spaces with Closed Null One-Form. *J. Math. Phys.* **2023**, *64*, 022502. [CrossRef]
138. Heefer, S. Berwald m-Kropina Spaces of Arbitrary Signature: Metrizability and Ricci-Flatness. *J. Math. Phys.* **2024**, *65*, 122502. [CrossRef]
139. Barthel, W. Zum Inhaltsbegriff in der Minkowskischen Geometrie. *Math. Z.* **1953**, *58*, 358. [CrossRef]
140. Barthel, W. Über eine Parallelverschiebung mit Längeninvarianz in lokal-Minkowskischen Räumen I, II. *Arch. Der Math.* **1953**, *4*, 346. [CrossRef]
141. Ingarden, R.S.; Tamássy, L. The Point Finsler Spaces and Their Physical Applications in Electron Optics and Thermodynamics. *Math. Comput. Model.* **1994**, *20*, 93. [CrossRef]
142. Nazim, A. *Über Finslersche Räume*; Dissertatio: München, Germany, 1936.
143. Varga, O. Zur Herleitung des Invarianten Differentials in Finslerschen Räumen. *Monatshefte Math. Phys.* **1941**, *50*, 165. [CrossRef]
144. Harko, T. Thermodynamic Interpretation of the Generalized Gravity Models with Geometry–Matter Coupling. *Phys. Rev. D* **2014**, *90*, 044067. [CrossRef]
145. Bertolami, O.; Böhmer, C.G.; Harko, T.; Lobo, F.S.N. Extra Force in $f(R)$ Modified Theories of Gravity. *Phys. Rev. D* **2007**, *75*, 104016. [CrossRef]
146. Harko, T.; Lobo, F.S.N.; Otalora, G.; Saridakis, E.N. Nonminimal Torsion–Matter Coupling Extension of $f(T)$ Gravity. *Phys. Rev. D* **2014**, *89*, 124036. [CrossRef]
147. Parker, L. Particle Creation in Expanding Universes. *Phys. Rev. Lett.* **1968**, *21*, 562. [CrossRef]
148. Parker, L. Quantized Fields and Particle Creation in Expanding Universes. I. *Phys. Rev.* **1969**, *183*, 1057. [CrossRef]
149. Zeldovich, Y.B.; Starobinsky, A.A. Particle Production and Vacuum Polarization in an Anisotropic Gravitational Field. *Zh. Eksp. Teor. Fiz.* **1971**, *61*, 2161, *Sov. Phys. JETP* **1972**, *34*, 1159.
150. Parker, L. Particle Creation in Isotropic Cosmologies. *Phys. Rev. Lett.* **1972**, *28*, 705, Erratum: *Phys. Rev. Lett.* **1972**, *28*, 1497. [CrossRef]
151. Fulling, S.A.; Parker, L.; Hu, B.L. Conformal Energy-Momentum Tensor in Curved Spacetime: Adiabatic Regularization and Renormalization. *Phys. Rev. D* **1974**, *10*, 3905. [CrossRef]
152. Parker, L. Particle Creation and Particle Number in an Expanding Universe. *J. Phys. A Math. Theor.* **2012**, *45*, 374023. [CrossRef]
153. Prigogine, I.; Geheniau, J.; Gunzig, E.; Nardone, P. Thermodynamics of Cosmological Matter Creation. *Proc. Natl. Acad. Sci. USA* **1988**, *85*, 7428. [CrossRef]
154. Calvão, M.O.; Lima, J.A.S.; Waga, I. On the Thermodynamics of Matter Creation in Cosmology. *Phys. Lett. A* **1992**, *162*, 223. [CrossRef]
155. Su, J.; Harko, T.; Liang, S.-D. Irreversible Thermodynamic Description of Dark Matter and Radiation Creation During Inflationary Reheating. *Adv. High Energy Phys.* **2017**, *2017*, 7650238. [CrossRef]
156. Lima, J.A.S.; Baranov, I.P. Gravitationally Induced Particle Production: Thermodynamics and Kinetic Theory. *Phys. Rev. D* **2014**, *90*, 043515. [CrossRef]
157. Saridakis, E.N.; González-Díaz, P.F.; Sigüenza, C.L. Unified Dark Energy Thermodynamics: Varying w and the -1-Crossing. *Class. Quantum Gravity* **2009**, *26*, 165003. [CrossRef]
158. Bernardo, J.M. Reference Prior Distributions for Bayesian Inference. *J. R. Stat. Soc. B* **1979**, *41*, 113–127. [CrossRef]

159. Joyce, J. Bayes' Theorem. In *The Stanford Encyclopedia of Philosophy*, Fall 2021 ed.; Zalta, E.N., Ed.; Stanford University: Stanford, CA, USA, 2021.
160. Foreman-Mackey, D.; Hogg, D.W.; Lang, D.; Goodman, J. emcee: The MCMC Hammer. *Publ. Astron. Soc. Pac.* **2013**, *125*, 306. [CrossRef]
161. Foreman-Mackey, D.; Hogg, D. W.; Lang, D.; Goodman, J. emcee v3: A Python Ensemble Sampling Toolkit for Affine-Invariant MCMC. *arXiv* **2019**, arXiv:1911.07688. [CrossRef]
162. Lewis, A. GetDist: A Python Package for Analysing Monte Carlo Samples. *arXiv* **2019**, arXiv:1910.13970.
163. Jimenez, R.; Loeb, A. Constraining Cosmological Parameters Based on Relative Galaxy Ages. *Astrophys. J.* **2002**, *573*, 37–51. [CrossRef]
164. Moresco, M.; Verde, L.; Pozzetti, L.; Jimenez, R.; Cimatti, A. Cosmological Constraints from Cosmic Chronometers: A New Approach. *J. Cosmol. Astropart. Phys.* **2012**, *2012*, 053. [CrossRef]
165. Moresco, M. Raising the Bar: New Constraints on the Hubble Parameter with Cosmic Chronometers at $Z \sim 2$. *Mon. Not. R. Astron. Soc.* **2015**, *450*, L16–L20. [CrossRef]
166. Moresco, M.; Pozzetti, L.; Cimatti, A.; Jimenez, R.; Maraston, C.; Verde, L.; Thomas, D.; Citro, A.; Tojeiro, R.; Wilkinson, D. A 6% Measurement of the Hubble Parameter at $Z \sim 0.45$: Direct Evid. Epoch Cosm. Re-Acceleration. *J. Cosmol. Astropart. Phys.* **2016**, *2016*, 014. [CrossRef]
167. Moresco, M.; Jimenez, R.; Verde, L.; Pozzetti, L.; Cimatti, A.; Citro, A. Cosmic Chronometers at $Z \sim 2$: New Constraints Hubble Parameter. *Astrophys. J.* **2018**, *868*, 84. [CrossRef]
168. Moresco, M.; Jimenez, R.; Verde, L.; Cimatti, A.; Pozzetti, L. Setting the Stage for Cosmic Chronometers. II. Impact of Stellar Population Synthesis Models Systematics and Full Covariance Matrix. *Astrophys. J.* **2020**, *898*, 82. [CrossRef]
169. Brout, D.; Scolnic, D.; Popovic, B.; Riess, A.G.; Carr, A.; Zuntz, J.; Kessler, R.; Davis, T.M.; Hinton, S.; Jones, D.; et al. The Pantheon$^+$ analysis: Cosmological constraints. *Astrophys. J.* **2022**, *938*, 110. [CrossRef]
170. Astier, P.; Guy, J.; Regnault, N.; Pain, R.; Aubourg, E.; Balam, D.; Basa, S.; Carlberg, R.; Fabbro, S.; Fouchez, D.; et al. The supernova legacy survey: Measurement of ω, ω and from the first year data set. *Astron. Astrophys.* **2006**, *447*, 31–48. [CrossRef]
171. Conley, A.; Guy, J.; Sullivan, M.; Regnault, N.; Astier, P.; Balland, C.; Basa, S.; Carlberg, R.; Fouchez, D.; Hardin, D.; et al. Supernova constraints and systematic uncertainties from the first three years of the supernova legacy survey. *Astrophys. J. Suppl. Ser.* **2010**, *192*, 1. [CrossRef]
172. Karim, M.A.; Aguilar, J.; Ahlen, S.; Alam, S.; Allen, L.; Prieto, C.A.; Alves, O.; Anand, A.; Andrade, U.; Armengaud, E.; et al. DESI DR2 Results II: Measurements of Baryon Acoustic Oscillations and Cosmological Constraints. *arXiv* **2025**, arXiv:2503.14738.
173. Pogosian, L.; Zhao, G.-B.; Jedamzik, K. Recombination-independent determination of the sound horizon and the Hubble constant from BAO. *Astrophys. J. Lett.* **2020**, *904*, L17. [CrossRef]
174. Jedamzik, K.; Pogosian, L.; Zhao, G.-B. Why reducing the cosmic sound horizon alone can not fully resolve the Hubble tension. *Commun. Phys.* **2021**, *4*, 123. [CrossRef]
175. Pogosian, L.; Zhao, G.-B.; Jedamzik, K. A consistency test of the cosmological model at the epoch of recombination using DESI BAO and Planck measurements. *Astrophys. J. Lett.* **2024**, *973*, L13. [CrossRef]
176. Lin, W.; Chen, X.; Mack, K.J. Early universe physics insensitive and uncalibrated cosmic standards: Constraints on Ω_m and implications for the Hubble tension. *Astrophys. J.* **2021**, *920*, 159. [CrossRef]
177. Vagnozzi, S. Seven hints that early-time new physics alone is not sufficient to solve the Hubble tension. *Universe* **2023**, *9*, 393. [CrossRef]
178. Chaudhary, H.; Csillag, L.; Harko, T. Semi-Symmetric Metric Gravity: A Brief Overview. *Universe* **2024**, *10*, 419. [CrossRef]
179. Cattoën, C.; Visser, M. Cosmographic Hubble fits to the supernova data. *Phys. Rev. D* **2008**, *78*, 063501. [CrossRef]
180. Visser, M.; Cattoën, C. Cosmographic analysis of dark energy. In *Dark Matter in Astrophysics and Particle Physics*; Klapdor-Kleingrothaus, H.V., Krivosheina, I.V., Eds.; World Scientific Publishing Co. Pte. Ltd.: Singapore, 2009; pp. 287–300.
181. Visser, M. Cosmography: Cosmology without the Einstein equations. *Gen. Relativ. Gravit.* **2005**, *37*, 1541. [CrossRef]
182. Luongo, O. Cosmography with the Hubble parameter. *Mod. Phys. Lett. A* **2011**, *26*, 1459. [CrossRef]
183. Visser, M. Jerk, snap and the cosmological equation of state. *Class. Quantum Gravity* **2004**, *21*, 2603. [CrossRef]
184. Andrae, R.; Schulze-Hartung, T.; Melchior, P. Dos and don'ts of reduced chi-squared. *arXiv* **2010**, arXiv:1012.3754.
185. Liddle, A.R. Information criteria for astrophysical model selection. *Mon. Not. R. Astron. Soc. Lett.* **2007**, *377*, L74. [CrossRef]
186. Vrieze, S.I. Model selection and psychological theory: A discussion of the differences between the Akaike information criterion (AIC) and the Bayesian information criterion (BIC). *Psychol. Methods* **2012**, *17*, 228. [CrossRef]
187. Tan, M.Y.J.; Biswas, R. The reliability of the Akaike information criterion method in cosmological model selection. *Mon. Not. R. Astron. Soc.* **2012**, *419*, 3292. [CrossRef]
188. Arevalo, F.; Cid, A.; Moya, J. AIC and BIC for cosmological interacting scenarios. *Eur. Phys. J. C* **2017**, *77*, 1. [CrossRef]
189. Burnham, K.P.; Anderson, D.R. *Model Selection and Multimodel Inference*, 2nd ed.; Springer: New York, NY, USA, 2010.
190. Jeffreys, H. *The Theory of Probability*; Oxford University Press: Oxford, UK, 1998.

191. Andrade, C. The P value and statistical significance: Misunderstandings, explanations, challenges, and alternatives. *Indian J. Psychol. Med.* **2019**, *41*, 210–215. [CrossRef]
192. Vargas, J.G.; Torr, D.G. The construction of teleparallel Finsler connections and the emergence of an alternative concept of metric compatibility. *Found. Phys.* **1997**, *27*, 825–843.
193. Tong, Y. General teleparallel gravity from Finsler geometry. *Commun. Theor. Phys.* **2023**, *75*, 095403. [CrossRef]
194. Amelino-Camelia, G. Quantum-Spacetime Phenomenology. *Living Rev. Relativ.* **2013**, *16*, 5. [CrossRef]
195. Caroff, S.; Pfeifer, C.; Bolmont, J.; Terzić, T.; Campoy-Ordaz, A.; Kerszberg, D.; Martinez, M.; Pensec, U.; Plaid, C.; Strišković, J.; et al. Discriminating between different modified dispersion relations from gamma-ray observations. *Phys. Rev. D* **2025**, *111*, 083021. [CrossRef]
196. Amelino-Camelia, G. Doubly special relativity. *Nature* **2002**, *418*, 34–35. [CrossRef]
197. Letizia, M.; Liberati, S. Deformed relativity symmetries and the local structure of spacetime. *Phys. Rev. D* **2017**, *95*, 046007. [CrossRef]
198. Majid, S.; Ruegg, H. Bicrossproduct structure of κ-Poincaré group and non-commutative geometry. *Phys. Lett. B* **1994**, *334*, 348–354. [CrossRef]
199. Amelino-Camelia, G.; Barcaroli, L.; Gubitosi, G.; Liberati, S.; Loret, N. Realization of doubly special relativistic symmetries in Finsler geometries. *Phys. Rev. D* **2014**, *90*, 125030. [CrossRef]

Disclaimer/Publisher's Note: The statements, opinions and data contained in all publications are solely those of the individual author(s) and contributor(s) and not of MDPI and/or the editor(s). MDPI and/or the editor(s) disclaim responsibility for any injury to people or property resulting from any ideas, methods, instructions or products referred to in the content.